

HST/WFPC2 imaging of the circumnuclear structure of LLAGNs. I Data and nuclear morphology¹

Rosa M. González Delgado¹, Enrique Pérez¹, Roberto Cid Fernandes², Henrique Schmitt³,

(1) Instituto de Astrofísica de Andalucía (CSIC), P.O. Box 3004, 18080 Granada, Spain
(rosa@iaa.es; eperez@iaa.es)

(2) Depto. de Física-CFM, Universidade Federal de Santa Catarina, C.P. 476, 88040-900,
Florianópolis, SC, Brazil (cid@astro.ufsc.br)

(3) Remote Sensing Division, Naval Research Laboratory, Code 7210, 4555 Overlook
Avenue, Washington, DC 20375 (hschmitt@ccs.nrl.navy.mil)

(4) Interferometrics, Inc., 13454 Sunrise Valley Drive, Suite 240, Herndon, VA 20171

ABSTRACT

In several studies of Low Luminosity Active Galactic Nuclei (LLAGNs), we have characterized the properties of the stellar populations in LINERs and LINER/HII Transition Objects (TOs). We have found a numerous class of galactic nuclei which stand out because of their conspicuous 0.1–1 Gyr populations. These nuclei were called "Young-TOs" since they all have TO-like emission line ratios. To advance our knowledge of the nature of the central source in LLAGNs and its relation with stellar clusters, we are carrying out several imaging projects with the Hubble Space Telescope (HST) at near-UV, optical and near-IR wavelengths. In this paper, we present the first results obtained with observations of the central regions of 57 LLAGNs imaged with the WFPC2 through any of the V (F555W, F547M, F614W) and I (F791W, F814W) filters that are available in the HST archive. The sample contains 34% of the LINERs and 36% of the TOs in the Palomar sample. The mean spatial resolution of these images is 10 pc. With these data we have built an atlas that includes structural maps for all the galaxies, useful to identify compact nuclear sources and, additionally, to characterize the circumnuclear environment of LLAGNs, determining the frequency of dust and its morphology. The main results obtained are: 1) We have not found any correlation between the presence of nuclear compact sources and emission-line type. Thus, nucleated LINERs are as frequent as nucleated TOs. 2) The nuclei of "Young-TOs" are brighter than the nuclei of "Old-TOs" and LINERs. These results confirm our previous results that Young-TOs are separated from

other LLAGNs classes in terms of their central stellar population properties and brightness. 3) Circumnuclear dust is detected in 88% of the LLAGNs, being almost ubiquitous in TOs. 4) The dust morphology is complex and varied, from nuclear spiral lanes to chaotic filaments and nuclear disk-like structures. Chaotic filaments are as frequent as dust spirals; but nuclear disks are mainly seen in LINERs. These results suggest an evolutionary sequence of the dust in LLAGNs, LINERs being the more evolved systems and Young-TOs the youngest.

Subject headings: galaxies:active – galaxies:nuclei – galaxies:clusters – galaxies:structure – dust, extinction

1. Introduction

Low-luminosity active galactic nuclei (LLAGNs) comprise 30% of all bright galaxies ($B \leq 12.5$) and are the most common type of AGN (Ho, Filippenko & Sargent 1997a, hereafter HFS97). These include LINERs, and transition-type objects (TOs, also called weak-[OI] LINERs). These two types of LLAGNs have similar emission line ratios in $[OIII]/H\beta$, $[NII]/H\alpha$, and $[SII]/H\alpha$, but $[OI]/H\alpha$ is lower in TOs than in LINERs. LLAGNs constitute a rather mixed class and different mechanisms have been proposed to explain the origin of the nuclear activity, including shocks, and photoionization by a non-stellar source, by hot stars or by intermediate age stars (e.g. Ferland & Netzer 1983; Filippenko & Terlevich 1992; Binnette et al. 1994; Taniguchi, Shioya & Murayama 2000). Because we do not know yet what powers them and how they are related to the Seyfert phenomenon, LLAGNs have been at the forefront of AGN research since they were first systematically studied by Heckman (1980). Are they all truly “dwarf” Seyfert nuclei powered by accretion onto nearly dormant supermassive black holes (BH), or can some of them be explained at least partly in terms of stellar processes? If LLAGNs were powered by a BH, they would represent the low end of the AGN luminosity function in the local universe and would also establish a lower limit to the fraction of galaxies containing massive BHs in their centers. If, on the contrary, LLAGNs were powered by nuclear stellar clusters, their presence would play an important role in the evolution of galaxy nuclei. Therefore, it is fundamental to unveil the nature of the central source in LLAGNs.

¹Based on observations with NASA/ESA *Hubble Space Telescope* obtained at the Space Telescope Science Institute, which is operated by the Association of Universities for Research in Astronomy, Inc., under NASA contract NAS 5-2655.

There is clear evidence that at least some LINERs harbor a bona fide AGN, and they may be considered the faint end of the luminosity function of Seyfert galaxies. It has been found that about 20% of the nearby LINERs have a weak broad H α emission component similar to those found in type 1 Seyferts (Ho, Filippenko & Sargent 1997b). In a few of these LINERs the H α line shows a double peak component (e.g. Storchi-Bergmann et al. 1997; Shields et al. 2000; Ho et al. 2000) suggesting that they are powered by an accreting black hole (BH). It has also been found that X-ray emission in LINERs has a nonthermal origin associated with an AGN (e.g. Terashima, Ho & Ptak 2000). Recent works based on higher spatial resolution data taken with Chandra show that only in half of the LLAGNs observed the X-ray emission is associated with compact nuclear cores (Satyapal et al. 2004; Dudik et al. 2006; González-Martín et al. 2006). This is consistent with VLA radio observations, which detect unresolved radio cores in half of the LINERs (Nagar et al. 2000, 2002). Finally, a monitoring study at near-UV wavelengths by Maoz et al. (2005) finds UV variability in a significant fraction of the 17 LLAGNs observed. The variation of the UV fluxes may be interpreted as the manifestation of low rate or low radiative efficiency accretion onto a supermassive BH.

On the other hand, detection of stellar wind absorption lines in the ultraviolet spectra of some TOs (Maoz et al. 1998; Colina et al. 2002) has proven unequivocally the presence of young stellar clusters in the nuclear region. Additional evidence comes from optical studies, in which we have focused on the study of the stellar population in the nuclei and circum-nuclear region of LLAGNs to establish the role of stellar processes in their phenomenology. Ground-based (Cid Fernandes et al. 2004; Cid Fernandes et al. 2005) and HST+STIS spectra (González Delgado et al. 2004) have shown that the contribution of an intermediate age stellar population is significant in a sizable fraction of the TO population. These studies identified a class of objects, called “Young-TOs”, which are clearly separated from LINERs in terms of the properties and spatial distribution of the stellar populations. They have stronger stellar population gradients, a luminous intermediate age stellar population concentrated toward the nucleus (~ 100 pc) and much larger amounts of extinction than LINERs. These objects, which underwent a powerful star formation event ~ 1 Gyr ago, could correspond to post-Starburst nuclei or to evolved counterparts of the Seyfert 2 with a composite nucleus, characterized too by harboring nuclear starbursts (González Delgado et al. 2001; Cid Fernandes et al. 2001, 2004). HST imaging of the nuclei of these Seyfert 2 galaxies shows that the UV emission is resolved into stellar clusters (González Delgado et al. 1998) that are similar to those detected in starburst galaxies (Meurer et al. 1995).

Nuclear stellar clusters are a common phenomenon in spirals, having been detected in 50-70% of these sources (Carollo et al. 1998, 2002; Boeker et al. 2002, 2004). Therefore stellar clusters are a natural consequence of the star formation processes in the central

region of spirals. On the other hand, evidence has been accumulating during the past few years about the ubiquity of BH in the nuclei of galaxies. Furthermore, the tight correlation of the BH mass and stellar velocity dispersion (Ferrarese & Merrit 2000; Gebhardt et al. 2000) implies that the creation and evolution of a BH is intimately connected to that of the galaxy bulge. Recently, in a HST survey in the Virgo Cluster, Côté et al. (2006) have detected compact sources in a comparable fraction of elliptical galaxies. These compact stellar clusters, referred to as nuclei by the authors (see also Ferrarese et al 2006a), have masses that scale directly to the galaxy mass, in the same way as do the BH masses in high luminosity galaxies (Ferrarese et al. 2006b). Therefore, a natural consequence of the physical processes that formed present-day galaxies should be the creation of a compact massive object in the nucleus, either a BH and/or a massive stellar cluster.

To determine the nature of the nuclear source of active galaxies and their evolution we are carrying out several projects with HST+ACS imaging at the near-UV wavelengths a sample of Seyferts (ID. 9379, PI. Schmitt, Muñoz-Marín et al. 2007) and LLAGNs (ID. 10548, PI. González Delgado). These observations are complemented with WFPC2 optical data retrieved from the HST archive. The high angular resolution provided by HST is crucial to determine the physical properties of the nuclei, the central structure of these galaxies, as well as to study the circumnuclear environment of AGNs. The main goals of these studies are to determine the frequency of nuclear and circumnuclear stellar clusters in AGNs, and whether they are more common in Seyferts, TOs or LINERs; to characterize the intrinsic properties of these clusters and to study whether there is evolution from Seyferts to TOs and LINERs. In addition, the frequency of dust and its morphology can also provide relevant information about the origin of nuclear activity. Dust is a valuable probe of the presence of cold interstellar gas in galaxies, and it is very sensitive to the perturbations that drive the gas toward the center and feed the AGN. Here, we present the initial results obtained for LLAGNs based on archival visible and red images obtained with the WFPC2. The paper is organized as follows: section 2 presents the sample selection, and 3 the characteristics of the observations. Sections 4, 5 and 6 describe the imaging atlas, the dust morphology and the central properties of the galaxies. Finally, the summary and conclusions are presented in section 7.

2. Galaxy Sample

The objects selected for this study are drawn entirely from the HFS97 catalog as it comprises the most complete and homogeneous survey of LINERs and TOs available for the local universe. Of the 160 galaxies classified as LLAGNs, we have already studied the

circumnuclear stellar population for about half of the HFS97 catalog (Cid Fernandes et al. 2004; González Delgado et al. 2004; Cid Fernandes et al. 2005; hereafter Papers I, II and III, respectively). These galaxies constitute the raw sample for this study. We have found suitable WFPC2 archival images for 57 of them, i.e. 36% of the original HFS97 LLAGNs sample.

Following the HFS97 emission-line classification, our subset contains 32 LINERs ($[\text{OI}]/\text{H}\alpha > 0.17$) and 25 TOs ($[\text{OI}]/\text{H}\alpha \leq 0.17$), i.e., 34 and 38% of whole HFS97 LLAGN sample, respectively. In Paper I we proposed a slight modification of this criterion, setting the LINER/TO dividing line at $[\text{OI}]/\text{H}\alpha = 0.25$. According to this definition, to be used throughout the rest of this paper, our sample includes 36% of the TOs and 34% of the LINERs in the HFS97 catalog. Figure 1 shows the morphological type, distance and $[\text{OI}]/\text{H}\alpha$ distributions of our sample as compared with the full HFS97 sample. The objects studied here generally follow the same distributions that the HFS97 sample. In our sample, the mean distance is 17 Mpc for the weak-[OI] ($[\text{OI}]/\text{H}\alpha \leq 0.25$) and 30 Mpc for the strong-[OI] ($[\text{OI}]/\text{H}\alpha > 0.25$) sources. The corresponding values in the whole HFS97 LLAGNs sample are 23 Mpc and 28 Mpc. The median morphological types in both samples are S0 and Sab for strong and weak-[OI], respectively.

Table 1 lists the main properties for the galaxies selected, such as emission spectral type, Hubble type, distance, and stellar population classification. The emission-line class, Hubble type and distance are from HFS97. These authors adopted the Hubble type from the RC3 (de Vaucouleurs et al 1991), and the distance from Tully (1988) for galaxies closer than 40 Mpc. For farther galaxies they derive distances simply from their radial velocities and $H_0 = 75 \text{ km s}^{-1} \text{ Mpc}^{-1}$. The properties related to the stellar population are from papers I and II. Following these papers, systems are classified as Young (Y) or Old (O) based on the detection of intermediate age stellar population features and the value of the equivalent width of the CaII K absorption band. Y nuclei always have $W_K \leq 15 \text{ \AA}$. Most of the O-nuclei have $W_K > 15 \text{ \AA}$, however, there are four LINERs, NGC 3998, NGC 4143, NGC 4203, and NGC 4450, that have old nuclear stellar populations but the CaII lines are diluted due to the AGN contribution, and thus they violate the $W_K > 15 \text{ \AA}$ rule for O systems.

In terms of combined emission ($[\text{OI}]/\text{H}\alpha$) and stellar population classifications, the current subsample comprises 17 Young-TOs, 20 Old-TOs, 18 Old-LINERs and 2 Young-LINERs. As we have found previously, \sim half of the TOs have young ($\leq 1 \text{ Gyr}$) populations, and almost no LINER has young stars.

3. Observations and data processing

The data collected for our subset of LLAGNs were all obtained with the WFPC2 on board of HST at optical wavelengths through any of these filters: F555W, F547W, F606W, F791W and F814W. The first three filters are a proxy for the visual V band, and the last two filters for the red broad I band. Table 2 lists for each galaxy the filters, the exposure times, and the image spatial scale of the observations, and the proposal identification number. Most of the galaxies were observed through one of the filters close to the V band, while three galaxies (NGC 4435, NGC 4438 and NGC 7331) have been observed only with the I band filters. Most of the galaxies (86%) were imaged with their centers in the high-resolution Planetary Camera (PC) CCD of the WFPC2, thus with a spatial sampling of 0.0456 arcsec/pixel, and a field of view of 36×36 arcsec. The remaining 8 galaxies were observed with a sampling of 0.1 arcsec/pixel and a field of view of 1.3×1.3 arcmin. Observations in both I and V equivalent filters are available for 60% of the sample, and for 40% of the galaxies we have a color image (V-I) with the high spatial sampling of 0.0456 arcsec/pixel.

The images were all processed by the standard WFPC2 pipeline developed at the STScI that corrects for flat-field and bias subtraction. When multiple exposures are available for the same target, the frames were combined and cosmic-ray cleaned in a single step using the IRAF/STSDAS task `crrej`, otherwise cosmic rays were removed using the task `cosmicrays` in the IRAF² package. For each frame, the cosmic-ray events were defined as pixels deviating by more than 5 sigma above the background and they were replaced by the average of several neighboring pixels. We have checked that the nucleus was not compromised by the cosmic ray rejection algorithm, i.e. removing flux that really corresponds to the nucleus; this could happen if the central surface brightness increases very rapidly in the central 2-3 pixels. To check this in the case of a single exposure, we have compared the number counts and the surface brightness profiles through the maximum number count pixel before and after the cosmic ray algorithm was applied. If the image results from the combination of several frames, we compare the surface brightness of the individual frames between them and with the resulting combined image.

The sky background of the images was estimated measuring in the outer part of the mosaiced WFPC2 image. We did not attempt to subtract it because most of the galaxies are extended well beyond the WFPC2 field of view; thus, this measurement provides a value higher than the actual sky background. We checked that for most of the galaxies these measurements, even though higher than the expected sky background, are low enough to

²IRAF is distributed by the National Optical Astronomical Observatory, which is operated by AURA, Inc., under contract to the NSF.

have a negligible effect on the measurements corresponding at least to the central 5 arcsec derived with no sky subtraction.

Photometric calibration was obtained using the zero point provided by the PHOTFLAMB key-word in the image header. PHOTFLAMB is the flux of a source with constant flux per unit wavelength which produces a count rate of 1 DN/s. For a given filter, the PHOTFLAMB values for most of the data are quite similar, and the differences between them is less than 1%. However, a few images have been observed with a gain equal to 15 e⁻/DN, instead of 7 e⁻/DN. For these images, the PHOTFLAMB is almost a factor 2 larger than for the rest of the galaxies that were observed with gain equal to 7 e⁻/DN. We have checked that the PHOTFLAMB values are in agreement with the value of this parameter provided by the package synphot. We use the expression $-2.5 \times \log(\text{counts/s} \times \text{PHOTFLAMB}) - 21.1$ to calculate the magnitudes in the STMAG system.

For the filters used in this work, this method provides zero points that are equivalent to the zero points calculated as $Z_{STMAG} + 2.5 \times \log GR_i + 0.1$ proposed by Holtzman et al (1995). The Z_{STMAG} is the synthetic zero points tabulated in table 9 of Holtzman et al (1995); GR_i is the gain ratio (so, $GR_i = 2$ for gain=7 e⁻/DN and $GR_i = 1$ for gain= 15 e⁻/DN). Note that the Holtzman et al (1995) zero points are derived using apertures of 0.5 arcsec, but the PHOTFLAMB are referred to counts measured with an infinite aperture. Because the infinite aperture is defined as having 1.096 times the flux in an aperture with 0.5 arcsec, we need to add 0.1 mag to the Z_{STMAG} to correct to infinite aperture.

Correction for Galactic extinction was performed using the E(B–V) values given in the NED³ following Schlegel et al (1998), and with the Cardelli et al. (1989) reddening law with $R_V = 3.1$.

4. The atlas, colors and the structure maps

An atlas of our sample is presented in Figure 2. For each galaxy, we show the V equivalent image in three scales, the full PC frame (when available, or the central ± 50 arcsec of the mosaiced image when the nucleus is not in the PC chip), a zoom into the central ± 4 arcsec, and the central ± 10 arcsec of the median filtered contrast image. The galaxies display a significant variety of morphologies. A brief description of the morphological features are given in Table 3. The description indicates the dust classification, the incidence of nuclear

³The NASA/IPAC Extragalactic Database (NED) is operated by the Jet Propulsion Laboratory, California Institute of Technology, under contract with the National Aeronautics and Space Administration.

sources and other features. The criteria for the dust classification and for determining whether a galaxy has a nuclear source are further explained in sections 5 and 6, respectively.

The V-I color image for 32 galaxies is also available, and in 23 of these galaxies the color map is sampled with 0.0456 arcsec/pixel. Color images are displayed in Figure 3.

There are several ways to map the circumnuclear dust in galaxies, each with its own advantages and caveats. In early type galaxies in which the central light distribution is well reproduced by elliptical isophotes, the structure map is obtained simply subtracting the model fit from the original image. The resulting image enhances the small deviation of the dust fine structural features from the isophotal model. This technique has been applied very often; some recent results obtained with HST images are, for example, those of Lauer et al. (2005). However, this technique can not be applied to all types of galaxies, since many of them show central isophotes that clearly deviate from an elliptical model. We were able to obtain suitable isophotal fits for some of the galaxies in the sample. The results of these models will be discussed in a forthcoming paper (González Delgado et al. 2007, in preparation).

Color images can also map the circumnuclear dust; for example, Ferrarese et al (2006a) use g-z color for galaxies in the Virgo cluster. Ideally, the color image must be obtained with two bands widely separated in wavelength, and with the same spatial resolution. This technique have been succesfully used to determine the amount of internal reddening in early type galaxies, where the stellar population does not change by a significant amount, so all the color variations can be attributed to dust. However, this assumption no longer applies for late type galaxies, which can show significant stellar population variations in the nucleus. Since many of our galaxies are spirals and we have two band frames (V and I) are available for only $\sim 60\%$ of the sample, we do not attempt to estimate the internal reddening using this technique.

To be able to obtain a structural map for all the galaxies, we have adopted here the unsharp masking technique. The unsharp masked image is obtained by dividing the original frame by a smoothed version obtained with a 31×31 median boxcar kernel. The structural maps are displayed, together with the original frames, in Figure 2. The dust structures are shown as dark regions in the maps; bright regions are locations of emission lines, if the filter includes emission lines, or enhanced stellar light. This technique gives similar results to that proposed by Pogge & Martini (2002) which is based on the Richardson-Lucy image restoration process (Richardson 1972; Lucy 1974), and it has been recently investigated by Simoes Lopes et al. (2007).

A comparison between the similarities and differences of the structural maps obtained

with the unsharp masking technique, the residual image resulting by subtracting an isophotal model, and the color image are displayed in Figure 4 for the galaxy NGC 3489. The main difference arises from the sharp increases of surface brightness of the central light. Note, however, these unsharp images are used mainly for the dust classification and not to find out whether a galaxy has a nuclear source.

5. The circumnuclear dust

HST observations of the central regions of galaxies have provided significant results with respect to the detection of dust, its morphology and its role in AGN. In fact, dust provides indirect evidence of the presence of cold interstellar gas and the mechanisms that drive the gas to the nucleus and fuel the AGN. Circumnuclear dust is common in Seyfert galaxies (e.g. Malkan, Gorjian & Tran 1998; Martini & Pogge 1999; Regan & Mulchaey 1999; Pogge & Martini 2002). Nuclear dust spirals are detected in many Seyfert galaxies. It has been argued that they trace the paths followed by the gas in its way to feed the AGN. A more recent study by Martini et al. (2003) has confirmed the ubiquity of dust at the center of Seyfert galaxies, with only 3% of these galaxies not having nuclear dust structures detected. These authors also find other dust morphologies in Seyfert galaxies, which are less structured and more chaotic than the nuclear spirals. Circumnuclear dust is also a common feature in radio galaxies (Verdoes Kleijn & Zeeuw 2005) and early type galaxies (Tran et al. 2001; Lauer et al. 2005; Ferrarese et al 2006a). In particular, Lauer et al. (2005) have found that half of the galaxies in their sample of early types have nuclear dust features, but this fraction rises to 90% when they consider only the galaxies with emission lines (presumably associated with nuclear activity). This result has been recently confirmed by Simoes Lopes et al. (2007), who found that all the 34 early-type AGN hosts in their sample have circumnuclear dust, but dust is detected only in 26% of the early type non-active galaxies.

We have found that circumnuclear dust is also common in LLAGNs, since 88% of the galaxies in our sample display dust features. The morphology is quite diverse, from nuclear disks, to filaments and lanes chaotically distributed, to well organized nuclear spiral arms. Here the morphology is determined by eye inspections, independently carried out by three of the authors, following the classification criteria established by Martini et al. (2003) and Lauer et al. (2005). These criteria are complementary. Lauer et al. (2005) distinguish between nuclear rings and disks from other structures that they divide into spiral and chaotic. The Martini et al. (2003) classification, which is in some aspects an extension of the Lauer et al. (2005) scheme, divides the spiral class into three sub-classes: grand design nuclear spirals, tightly wound spirals, and loosely wound nuclear spirals. Note that these works

found significantly different results, that justify their complementary dust classification. For instance, Martini et al. (2003) do not find any nuclear disks in Seyfert galaxies, while in Lauer et al. (2005) the detection of nuclear spirals in early type galaxies is rare. However, here we detect a significant fraction of nuclear dust disks and different types of spiral dust structures. Thus, we adopt the following criteria for the classification:

- *Grand Design Nuclear Spiral (GD)*. Galaxies belonging to this class have two symmetric dust spiral arms. They are similar to the grand design spirals but in spatial scales of less than a kiloparsec. Only two (NGC 841, NGC 3705) of the LLAGNs of our sample belong to this class (4% of the sample).
- *Tightly Wound Nuclear Spiral (TW)*. Galaxies with nuclear dust spirals with small pitch angles. They lack the symmetry of the grand design class, and represent 19% of the sample. One example of this class is NGC 4736.
- *Loosely Wound Nuclear Spiral (LW)*. These have a coherent nuclear spiral structure but with large pitch angle. One example is NGC 6951. This class is \sim as common as the TW class, with 14% of our sample belonging to it.
- *Chaotic Nuclear Spiral (CS)*. These galaxies show fragments of dust arcs that suggest a spiral structure. Galaxies belonging to this class may represent objects in a transition phase between the spiral and the chaotic class. Examples of this class are NGC 3368 and NGC 3169, with 17% of the LLAGNs in this class.
- *Chaotic Circumnuclear Dust (C)*. These galaxies clearly show circumnuclear dust but they cannot be classified as spiral structures. In many of these galaxies the dust appears as filaments and lanes. 25% of the LLAGNs are in this class, one example is NGC 2685.
- *Disks and nuclear rings (D)*. They are circular and axisymmetric structures. NGC 315 and NGC 2787 are examples of galaxies belonging to this class. They represent 9% of the sample.
- *No dust structure (N)*. Galaxies with no dust in the circumnuclear regions. NGC 3998 is one example; 12% of LLAGNs do not show any circumnuclear dust.

Table 3 summarizes the description of the dust morphology obtained, and Table 4 compares the frequency of dust morphologies for the LLAGNs with the results for Seyferts and non-active galaxies. The most remarkable result is that dust is almost ubiquitous in LLAGNs. Only 12% of the galaxies of our sample do not display dust features. Dust is as

frequent as in Seyferts (Martini et al. 2003), but the distribution of the dust morphology is different. As mentioned above, most of the Seyferts have dust spirals or dust filaments and arcs chaotically distributed; the dust disk morphology and non-dusty class are quite rare, while LLAGNs display dust disk morphology.

Figure 5 shows the histogram of the circumnuclear dust of LLAGNs in the seven dust-classes discussed. Well organized nuclear dust spirals (GD+TW+LW) are as frequent as the chaotic dust features (CS+C), and they are both more often detected than the dust disk-like morphology. Figure 5 also displays the distribution of the circumnuclear dust classes for strong- and weak-[OI] LLAGNs, ie., LINERs and TOs. A significant differential result emerges. The fraction of objects with dusty disks or no dust is higher in LINERs than TOs, while the fraction of chaotic dust features is equal in both types. An even larger systematic difference appears dividing the sample into the Young and Old stellar population categories. No Young LLAGN falls in either the no-dust or dusty-disk classes. Old systems, on the other hand, span the full menu of dust morphologies (Figure 6).

The spectral analysis performed in Papers I–III strongly suggests that Young-TOs are dustier than other LLAGN. A qualitative inspection of the images and structure maps in our atlas reveals that dust features in these objects are indeed very strong, which provides direct confirmation that Young-TOs stand out among LLAGN in terms of their dust content.

Besides the morphology, we have also evaluated the dust concentration. We have classified the LLAGNs in three classes according with the detection of dust in the inner part, in the outer part or throughout. Thus, the dust is highly concentrated if it is detected only in the central region within a radius $\leq 100\text{--}200$ pc, which at the mean distance of the objects corresponds to 1–2 arcsec radius. Dust concentration is graded by *in*, *out* or *inout* if the dust is detected at shorter distances (radius $\leq 100\text{--}200$ pc), only at larger distances or at both, respectively. We find that in most cases dust is distributed inside and outside of the central 100–200 pc radius. We have not found any difference in the dust concentration distribution in weak-[OI] and strong-[OI] LLAGNs. Dust located only in the inner part is equally frequent in TOs than in LINERs. However, the fraction of LLAGNs that have the dust located only in the inner part is larger in Old-systems (Old-TOs and LINERs) than in Young-systems (mainly Young-TOs). For most of the Young-TOs the dust is located throughout.

Lauer et al. (2005) and Ferrarese et al. (2006a) have proposed that the different dust morphologies in early type galaxies indicate a dust-settling evolutionary sequence. According to these authors, dust would be initially distributed in chaotic and non-ring structures, then it would sink to the center forming a disk or a ring, and finally be destroyed. The results obtained here suggest too an evolutionary sequence of the dust in these galaxies. If LLAGNs are part of this sequence, LINERs are more evolved systems than TOs because the fraction

of objects with disks or non-dust detection is significantly higher in the former type. This sequence is also in agreement with the difference of nuclear stellar population results found for these two types of LLAGNs (papers I and II). We found that strong-[OI] LLAGNs are mainly characterized by an old stellar population at the nucleus, but half of the weak-[OI] LLAGNs are dominated by an intermediate stellar population (our Young-TO class). In these works we suggest too an evolutionary sequence from Young-TOs to Old-LINERs.

Other interesting differential results are also found dividing our LLAGN sample in early (S0+E) and late (spirals) Hubble-types. Dust is almost ubiquitous in spirals, but not detected in 24% of the early type LLAGN hosts. This result is not totally in agreement with those obtained by Simoes Lopes et al (2007), since they found that all the early type AGN hosts of their sample have circumnuclear dust. Additionally, we have found that the dust disk morphology is only present in early type LLAGNs (see Table 4).

6. Properties of the galaxy center

6.1. Central magnitude and surface brightness

To determine the central magnitude we have performed circular aperture photometry using the task `phot` in the IRAF package SYNPHOT. Although the better way to measure the magnitudes of the galaxies would be by fitting ellipses to the images, this could only be done for $\sim 40\%$ of the sample. Since the nuclear regions of most galaxies are disturbed by dust or have a complicated stellar population distribution, they cannot be properly fitted by ellipses. Given these limitations, in order to obtain a consistent set of measurements for all galaxies we decided to use circular apertures. The apertures are centered at the maximum brightness, which is determined as the centroid of the central $5'' \times 5''$. This criterium is not applied for galaxies that have the center totally obscured by dust lanes. In these cases, the centroid is calculated with a larger number of central pixels, or it is taken as the center of external isophotes which are not much affected by the dust lanes. The integrated count rates are converted to ST magnitudes using the PHOTFLAMB parameter of the image header as explained in section 3. These central magnitudes are corrected for Galactic extinction as described in Section 3. Table 5 lists the central magnitudes measured with apertures of 0.2, 0.5 and 1 arcsec radius in the filters F547M, F555W, F606W and F814W. These quantities have not been corrected for sky background; the reason is that most galaxies in the sample extend beyond the WFPC2 FOV and thus the sky background can not be determined properly. However these central quantities are not affected significantly by the sky background. In fact, for those galaxies that are smaller than the WFPC2 FOV, we have checked that the difference between the central magnitude corrected and uncorrected for

background is much less than 0.01 magnitude. Note that these magnitudes correspond to integrated values, including the contribution from the stars and an AGN component when present, which have not been corrected for internal dust obscuration.

Additionally, the surface brightness (μ) at several distances (0.2, 0.5 and 1 arcsec) from the centroid is also calculated for each galaxy and listed in Table 5. The approach is to extract the mean number of counts in a circular annulus and then convert it to magnitudes per arcsec². The measurements are performed in a sequence of circular apertures of radii increasing in 1 pixel. This method allows us to derive a surface brightness profile, and to estimate μ at any distance. As for the central magnitudes, we have not corrected μ for internal dust obscuration.

One important uncertainty in the determination of the central magnitude and surface brightness, in particular the measurements at 0.2 arcsec, comes from the determination of the centroid of the maximum central emission. Several galaxies do not have a single central maximum, rather they show several knots produced by a patched central extinction or/and by the actual presence of several clusters. In these cases, the magnitude and surface brightness listed in Table 5 correspond to the measurements obtained placing the center of the aperture at the centroid of the brightest knot. Obviously, for these galaxies (NGC 660, NGC 841, NGC 3627, NGC 4192 and NGC 5005) the central 0.2 arcsec magnitude can be significantly different, by up to more than 0.1 mag, if the aperture is centered in another knot. However, the integrated magnitudes at 0.5 and 1 arcsec radius are not affected by the choice of the aperture center, even for those galaxies with several central knots. The central measurements of the galaxies that have a very obscured nucleus, such as NGC 2911, NGC 4150, NGC 3166, and NGC 7177, are affected by the choice of the galaxy center.

As expected, the galaxies that have been observed at F547M and at F555W show surface brightness profiles and magnitudes that are equal in both filters. The magnitudes and surface brightness profiles in the F606W filter can be slightly brighter than the same quantities measured in the F547M or F555W filters. Five galaxies (NGC 3169, NGC 3627, NGC 5005, NGC 5055 and NGC 6951) have been observed in F547M (or F555W) and F606W. Except for NGC 3627, the other four galaxies are brighter by about 0.1 mag in F606W than in F547M or F555W. This difference can be explained by the contribution of H α emission in F606W that does not affect F547M or F555W. Nuclear spectra of these galaxies show indeed H α in emission that can account for the small difference in magnitude between the two filters. Because this difference in the F606W and F555W (or F547M) magnitude is small, for statistical purposes we consider all three filters, F547M, F555W and F606W as equivalent to a visual magnitude.

Figure 7 shows the distribution of the magnitudes of the galaxies observed in any of the

F547M, F555W, or F606W filters. Table 7 shows the mean magnitude and surface brightness for all the objects and for those that fall into the categories of LINERs, TO, galaxies with central young/intermediate age population, and galaxies with old stellar population (following the W_K -based criterion explained in Section 1). Figure 7 and Table 7 indicate that LINERs and TO have similar central magnitudes and surface brightness in the F547M, F555W, or F606W bands. However, galaxies with central young/intermediate age populations are about 0.5 mag (or 0.5 mag/arcsec²) brighter than galaxies with central old stellar populations. Because we have not corrected these magnitudes by internal dust obscuration, the true difference in brightness is certainly *larger* than this, since these galaxies with central young/intermediate age populations are also dustier (Section 5, Paper III). From the spectral analysis carried out in Paper III, we find that the central regions of Young systems have, on average, A_V three times larger than Old systems (mean A_V of 0.6 and 0.2 mag, respectively). Therefore, correcting for internal dust would only strengthen this result.

In the F814W band, the surface brightness at 0.2 arcsec in sources with young/intermediate age populations is larger than in those with old stellar populations. These differences disappear when the surface brightness is measured at 1 arcsec. These results suggest that a fraction of the LLAGNs with young/intermediate age populations may have compact bright central sources.

6.2. Frequency of nuclear compact sources

HST observations have revealed that 50-70% of the spiral galaxies contain nuclear stellar clusters (Carollo et al 1998, 2002; Boeker et al 2002, 2004). Compact nuclear sources have also been detected by Côté et al (2006) and Ferrarese et al (2006a) in almost all early type galaxies in their survey, except in giant ellipticals. These compact sources are not associated with AGNs, and most of them are extended. Their colors suggest that they are clusters with old and intermediate age populations. Ferrarese et al (2006b) argue that they are low-mass counterparts of the BHs detected in bright elliptical galaxies.

Our goal here is to determine the frequency of nuclear compact sources in LLAGNs and identify possible differences between their sub-types. To determine the frequency of nucleated galaxies in LLAGNs can be a key point to determine the nature of TOs and LINERs, and the differences between both types of nuclear activity.

A compact light source is identified sometimes for rising above the inward extrapolated surface brightness cusp at small radii. For example, if the underlying galaxy is modeled by a Nuker law, then the nucleus is identified as an excess above the power law extrapolation

(e.g. Lauer et al. 1995, Ravindranath et al. 2001, Rest et al. 2001, Scarlata et al. 2004, Lauer et al. 2005, Hughes et al. 2005). However, Graham et al. (2003) and Trujillo et al. (2004) have shown that a Sérsic model (Sérsic 1968) can provide a better fit to the surface brightness profiles of early type galaxies, since a Nuker law is quite sensitive to the radial extent of the data. Recently, Ferrarese et al. (2006a) and Côté et al. (2006) have also shown that a Sérsic, or a core-Sérsic provide adequate fits to the whole surface brightness profile of elliptical galaxies in the Virgo cluster. This is actually a controversial topic, and arguments favoring the Nuker (Lauer et al. 2006) or the Sérsic models (Ferrarese et al. 2006c) have been given extensively during the last year.

In summary, an excess above the Nuker, Sersic or core-Sersic fits can be produced by a compact source. Note, however, that these methods are able to identify a bright compact source at the galaxy center, but do not determine the nature of the nuclear component, i.e., whether it is due to an AGN or a stellar cluster. If the source is extended, this nuclear component is probably related with stellar clusters. But, if the central source is spatially unresolved, and the central light excess is well fitted by a PSF, we can not say too much about the nature of the nucleated component. AGNs are expected to be point sources, but certainly many nuclear stellar clusters at the distance of these galaxies can be also unresolved (e.g. the nuclear cluster in NGC 4303, Colina et al. 2003). Due to these limitations, we propose to combine the morphology and surface brightness profile analysis together with the study of the nuclear stellar population properties of these objects (results already obtained in Papers I, II and III) to try to distinguish between the AGN or stellar cluster nature of the nuclear compact sources.

To identify whether a LLAGN has a compact source we have inspected the surface brightness profiles of these galaxies. We use the task 'ellipse' in STSDAS to fit isophotes. If the galaxy shows dust filaments, lanes or discs but the dust obscuration is not severe, we used the following approach. First, for each galaxy, the isophotes were constrained by fitting ellipses with a fixed center, ellipticity and position angle, chosen as the best fit to the apparent galaxy shape in the regions where dust is not present. A model image was then built with the task "bmodel" in STSDAS using the results from this first fit. This model image is subtracted from the data, producing a dust frame that is used later to correct the original image. A new fit is performed in the image corrected by dust, but now the center, ellipticity and position angle of each isophote were not constrained. The results for two galaxies with no dust (e.g. NGC 3998) or with a small amount of obscuration (e.g. NGC 6384) are shown in Figure 8. Other examples (NGC 2787 and NGC 5337) are in Figure 9. Here, the obscuration is larger but the dust is distributed mainly in only one side of the galaxy, and we are able to perform the fit to the undistorted part of the isophotes.

Unfortunately, many of the galaxies in this sample show non-elliptical isophotes, and/or the dust obscuration is severe (e.g. NGC 4150, NGC 7177), so that we are not able to fit their light distribution. Hence, the analysis of the surface brightness profile can not be the main method used to find out the fraction of LLAGNs that have compact sources; a different approach is needed to identify compact sources in these galaxies. We have identified nuclear compact sources by visual inspection of the HST images, as done by Carollo et al (1998). If a color image is available, we also inspect the color frame to check if a compact source with a color different from that of the underlying background is detected (see, for example, the F547M/F814W image of NGC 5055 in Fig 3). Additionally, we have built a surface brightness profile for all the galaxies of the sample by performing aperture photometry. We have checked that the profiles built in this way are quite similar to the profiles obtained using the task "ellipse" in STSDAS for the galaxies that are well fitted by elliptical isophotes (see the comparison for NGC 3998 and NGC 6384 in Figure 8). The agreement between the profiles obtained with the two processes is remarkable for most of the galaxies. Finally, for the objects that we identify visually a central source, we explore if the surface brightness also shows an inflexion point at small radii in the gradient profile. This gradient is obtained by calculating for each radius the slope of the profile. Figure 8 shows the gradient profile obtained for NGC 3998 and NGC 6384. Note, however, that by itself, an inflexion point in the light profile does not necessarily reflect the presence of a nuclear component because it can also be produced by varying dust obscuration.

Summarizing, we assume that the galaxy has a nuclear compact source if the following conditions are met: we visually identified this source in the image, and/or in the color image, in the surface brightness profile (built fitting ellipses to the isophotes and/or by aperture photometry) and by an inflexion point in the gradient profile at small radii. Table 4 lists the LLAGNs that have nuclear compact sources. Following Ferrarese et al (2006a), we call them nucleated galaxies. This table also mentions the objects that have several central sources. Usually these objects also show dust at the center, and in these cases it is difficult to know whether they are several real sources or a consequence of the dust distribution.

Table 7 summarizes the results of this analysis, indicating the frequency of LLAGNs that can be classified as nucleated, non-nucleated and those with several compact sources and central dust. The frequency of nucleated LLAGNs (51%) is similar to the fraction of spiral galaxies with nuclear stellar clusters (Carollo et al. 1998, 2002; Boeker et al 2002, 2004). This result is not unexpected since most (93%) of the LLAGNs are spirals. We do not find any significant difference in the frequency of nucleated strong- and weak-[OI] LLAGNs. However, the fraction of galaxies classified as Young-TOs that have compact nuclear sources (67%) is much higher than those that are non-nucleated (22%). Old-TOs, on the other hand, are somewhat more frequently non-nucleated (58%). LINERs host mainly old populations, and

they are equally frequent in the nucleated and non-nucleated categories. None of the only two LINERs classified as Young is classified as nucleated, but both show knots (presumably stellar clusters) and dust at the center.

To estimate the nuclear magnitude, we have first estimated the maximum radius of the nuclear component by inspecting the gradient profile and the inflexion point. Then, the magnitude was estimated by measuring the flux in a circular aperture of radius equal to the inflexion point (r_{in}). This flux is subtracted from the underlying galactic light contribution that is assumed to have equal surface brightness that the annulus of inner ($r_{in}+1$ pixel) and outer ($r_{in}+3$ pixels) radii. To estimate the uncertainty in the nuclear magnitude, we have estimated this quantity by changing r_{in} by ± 1 pixel, and by measuring the background light contribution in annuli of radii ($r_{in}, r_{in} + 2$) and ($r_{in} + 2, r_{in} + 4$). Table 8 lists r_{in} and the resulting measurements. This method to estimate the nuclear magnitude is similar to the method used by Carollo et al (1997), who fit the central source with a gaussian, and assume that the underlying galactic continuum light is represented by the asymptotic value of the gaussian wings. In fact, our results for the three galaxies (NGC 5377, NGC 5985 and NGC 6384) in common with the Carollo et al (1998) sample agree with their values. This method also provides similar (or lower) values to the nuclear magnitude estimated fitting the surface brightness profile with a King model (King 1968) for the central source plus a Sersic law for the underlying galaxy.

Figure 10 shows the distribution of the nuclear magnitudes and surface brightnesses of the nucleated galaxies observed in any of the V (F547M, F555W, F606W) filters divided into emission-line (LINERs and TO) and stellar-population groups. Despite the overlap, it is clear that, as for the central magnitudes studied in Section 6.1, Young systems are brighter. The average difference is about 2 mag in the nuclear surface brightness. Again, this should be considered a lower limit, since we have not corrected for internal extinction, and Young systems are dustier than Old ones. Furthermore, most of the galaxies known to have some contribution from the AGN to the nuclear component (NGC 315, NGC 3998, NGC 4203 and NGC 4261) are LINERs. If it were possible to take the AGN contribution into account, one would find a larger difference in the magnitudes of the nuclear stellar components.

In order to further investigate the nature of the nuclear components in this sample we compare our results with those from Chiaberge, Capetti & Macchetto (2005). These authors compared, in Figure 4 of their paper, the distribution of nuclear radio and optical luminosities of LINER's with those of FRI radio galaxies and Seyfert galaxies. They find that a small number of LINER's follow in the relation observed for Radio galaxies, indicating that in their case the nuclear component is due to synchrotron radiation at the base of the jet (Chiaberge et al. 1999). Two of the galaxies in our sample (NGC 315 and NGC 4261)

fall in this category. They also found that the remaining galaxies fall closer to the relation defined by Seyfert galaxies.

In Figure 11 we compare our galaxies with the Seyfert’s and LINER’s from Chiaberge et al. (2005)⁴. For simplicity we excluded the Radio Galaxies. Radio fluxes obtained from Nagar, Falcke, & Wilson (2005), and are presented in Table 7. These measurements were converted from 15 GHz to 5 GHz assuming a flat spectral index. We also converted the optical luminosities of our compact nuclear sources to $\lambda = 7000\text{\AA}$, the same wavelength used by Chiaberge et al. (2005), assuming a spectral index ν^{-1} . We can see in this Figure that in the case of TO’s, either Old or Young ones, 15 out of the 17 sources were not detected in radio. On the other hand only 1 of the 9 LINER’s was not detected.

The distribution of our sources in Figure 11 shows an interesting result. We find that the Old-LINER’s follow the relation defined by Seyfert galaxies, extending it to lower luminosities and suggesting that the nuclear component in these sources could be due to AGN emission. Further evidence in favor of this interpretation comes from the detection of broad H α emission in most of these sources (see Table 1) (Ho et al. 2000). In the case of TO’s, in particular the Young ones, their distribution is displaced relative to the relation defined by Seyferts and LINER’s. These galaxies have higher optical luminosities than what one would expect based on their radio luminosities. This result suggests that the source of the optical emission is different from that of Old-LINER’s, and most likely have a stellar origin, consistent with the spectroscopic results.

While a detailed interpretation of these findings is beyond the scope of this paper, we close this section with a speculation on a possible evolutionary scenario. Assuming TO nuclei to be stellar clusters, their detectability above the underlying background depends on its brightness, which, for a given mass, decreases with age⁵. Given the difficulties in identifying low contrast nuclei, it is likely that a cluster which is Young and detected now would fade beyond detection when it gets Old. Furthermore, as it ages, its color becomes more similar to that of the underlying old stellar population, and thus more difficult to be identified with our color criterion. Dust present at Young ages should tend to dissipate or settle onto a more organized structure. Between the age ranges typical of our Young

⁴Notice that Chiaberge et al. (2005) used the classification from Ho et al. 1997, which is slightly different from the one used here. As a result some of their galaxies (e.g. NGC404, NGC 3368, NGC 4314 and NGC 4736) should be considered TO’s.

⁵However, the level of detectability also depends on the surface brightness profile of the underlying galaxy. So, a compact source is more easily detected in a galaxy with a flat surface brightness profile than in one with a steep power law cusp.

and Old stellar-population categories (0.1–1 Gyr and 10 Gyr, respectively) a coeval stellar population fades by $\sim 2\text{--}4$ mag. The observed change in brightness will be smaller since extinction decreases with time. Using the typical 0.4 mag difference in A_V between Young and Old LLAGN estimated in Paper III, give brightness changes between 1.6 and 3.6 mag, depending on whether we use 1 or 0.1 Gyr to characterize the Young class. Needless to say, these are very rough numbers, but they do compare favorably with the average difference of ~ 2 mag in nuclear surface brightness between Young and Old systems.

A more detailed analysis should quantify the detectability threshold and take into account the ranges of masses and ages for such clusters, as well as the possibility that they have not been formed instantaneously (van der Marel et al. 2007). At present, however, this qualitative evolutionary scenario seems consistent with most of our findings.

7. Summary and Conclusions

LLAGNs, that include LINERs and TOs, are the most common type of AGN. What powers them is still at the forefront of AGN research. To unveil the nature of the central source we are constructing a panchromatic atlas of the inner regions of these galaxies, which will be used to determine their nuclear stellar population. To this end we have already carried out a near-UV snapshot survey of nearby LLAGNs with the ACS on board HST, that is complemented with optical and near-IR images available in the HST archive.

In this paper, the first of a series, we present observations of 57 LLAGNs imaged with the WFPC2 through any of the V (F555W, F547M, F606W) and/or I (F791W, F814W) bands. These objects comprise 36% of the original HFS97 LLAGNs sample, and correspond to those for which there are WFPC2 images available in the HST archive and whose circumnuclear stellar population we have already studied spectroscopically (Papers I–III). The subset of objects studied here follows the same distance and morphological type distribution of the complete HFS97 LLAGN sample. Classifying the objects in strong-[OI] and weak-[OI] ($[\text{OI}]/\text{H}\alpha \leq 0.25$), this subset includes 34% and 36% of the strong- and weak-[OI], respectively, of the whole HFS97 LLAGN sample. Following our results obtained from the analysis of the circumnuclear stellar population, this sub-sample contains 17 Young-TOs, 20 Old-TOs, 18 Old-LINERs and 2 Young-LINERs. Young-TOs or Young-LINERs are LLAGNs in which intermediate age stars contribute significantly to the nuclear blue-optical continuum. The dearth of Young-LINERs in the sample can be understood from the result obtained in our spectroscopic studies, which show that the overwhelming majority of LINERs harbor an old stellar population.

With these data we have built an atlas that includes the structural map for all the images, and color maps for those galaxies for which images in two filters are available. We have identified those galaxies that have nuclear compact sources, and we have studied the circumnuclear environment of LLAGNs. We have found circumnuclear dust in 88% of the LLAGNs, but this fraction is somewhat larger (95%) in weak-[OI] LLAGNs. The dust morphology is quite complex, from nuclear spiral lanes, to chaotic filaments and to nuclear disk-like structures. Chaotic filaments are as frequent as the well organized dust spirals; but disks are mainly seen in strong-[OI] LLAGNs. The dust concentration (simply graded by its location relative to a radius of 100-200 pc, is similar in weak- and in strong-[OI] because the fraction of LLAGNs with dust located only in the inner part is larger in Old-LLAGNs than in Young-LLAGNs. These results suggest an evolutionary dust sequence from Young-TOs to Old-LLAGNs.

We have found that LINERs and TOs have both similar central magnitude and surface brightness, but LLAGNs with young and intermediate age populations are brighter than Old-TOs and LINERs. We have not found any correlation between the presence of nuclear compact sources and the emission line spectral type, ie., LINERs are as frequently nucleated as TOs. However, the centers of Young-TOs are brighter than the centers of Old-TOs and LINERs. The difference in magnitude and surface brightness can be even larger if we account for internal extinction, since Young-TOs are dustier. This result indicates that Young-TOs are separated from other type of LLAGNs also in terms of their central brightness, in addition of the properties and spatial distribution of the stellar population.

These data have been very useful to study the circumnuclear environment of LLAGNs, and to identify which of these galaxies have a nuclear compact source. The fact that compact sources are as frequent in LINERs as in TOs, confirms again that LLAGNs are a mixed bag of objects. These results also suggest that the central morphology alone is not sufficient to elucidate the origin of their central source, and it cannot be used to ascertain whether LLAGNs are powered by AGNs or stellar clusters. These data will be complemented with near-UV (ACS) and near-IR (NICMOS) images to provide a panchromatic atlas of the inner regions of LLAGNs and to further investigate the origin of the nuclear sources and their relation with stellar clusters.

Acknowledgements We thanks the referee for her/his suggestions that helped to improve the paper. RGD and EP acknowledge support from the Spanish Ministerio de Educación y Ciencia through the grant AYA2004-02703. The data used in this work come from observations made with NASA/ESA Hubble Space Telescope, obtained from the STScI data archive. Basic research in radio astronomy at the NRL is supported by 6.1 base funding. We also thank support from a joint CNPq-CSIC bilateral collaboration grant.

REFERENCES

- Binette, L., Magris, C.G., Stasinska, G., & Bruzual, A.G. 1994, *A&A*, 292, 13
- Boeker, T., Laine, S., van der Marel, R.P., Sarzi, M., Rix, H.-W., Ho, L.C., & Shields, J.C. 2002, *AJ*, 123, 1389
- Boeker, T., Sarzi, M., McLaughlin, D.E., van der Marel, R.P., Rix, H.-W., Ho, L.C., & Shields, J.C. 2004, *AJ*, 127, 105
- Carollo, M., Stiavelli, M., de Zeeuw, P.T., & Mack, J. 1997, *AJ*, 114, 2366
- Carollo, M., Stiavelli, M., de Zeeuw, P.T., & Mack, J. 1998, *AJ*, 116, 68
- Carollo, M., Stiavelli, M., Seigar, M., de Zeeuw, P.T., & Dejonghe, H. 2002, *AJ*, 123, 159 2002
- Chiaberge, M., Capetti, A., & Celotti, A. 1999, *A&A*, 349, 77
- Chiaberge, M., Capetti, A., & Macchetto, F. D. 2005, *ApJ*, 625, 716
- Cid Fernandes, R., Heckman, T., Schmitt, H., González Delgado, R.M., & Storchi-Bergmann, T. 2001a, *ApJ*, 558, 81
- Cid Fernandes, R., González Delgado, R.M., Schmitt, H., et al. 2004a, 605, 105
- Cid Fernandes, R., Gu, Q., Melnick, J., Terlevich, E., Terlevich, R., Kunth, D., Rodrigues Lacerda, R., & Joguet, B. 2004b, *MNRAS*, 355, 273
- Cid Fernandes, R., González Delgado, R.M., Storchi-Bergmann, T., Martins, L.P., & Schmitt, H. 2005, *MNRAS*, 356, 270
- Colina, L., González Delgado, R.M., Mas-Hesse, J.M., & Leitherer, C. 2002, *ApJ*, 579, 545
- Côté, P., et al. 2006, *ApJS*, 165, 57
- de Vaucouleurs, G., de Vaucouleurs, A., Corwin, H. G., Jr., Buta, R. J., Paturel, G.; Fouque, P., 1991, *Third Reference Catalogue of Bright Galaxies* (New York: Springer) (RC3)
- Dudik, R.P., Satyapal, S., Gliozzi, M., & Sambruna, R.M. 2005, *ApJ*, 620, 113
- Ferrarese, L., & Merrit, D. 2000, *ApJ*, 539, L9
- Ferrarese, L., Côté, P., Jordán, A., et al. 2006a, *ApJS*, 164, 334
- Ferrarese, L., Côté, P., Dalla Bontà, E., et al. 2006b, *ApJ*, 644, 21
- Ferrarese, L., Côté, P., Blakeslee, J.P., Mei, S., Merrit, D., West, M.J. 2006c, (astro-ph/0612139)
- Ferland, G.J., & Netzer, H. 1983, *ApJ*, 264, 105
- Filippenko, A.V., & Terlevich, R. 1992, *AJ*, 397, 79
- Gebhardt, K., Kormendy, J., & Ho, L.C. 2000, *ApJ*, 539, L13

- González Delgado, R.M., Heckman, T., Leitherer, C., Meurer, G., Krolik, J., Wilson, A.S., Kinney, S., & Koratkar, A. 1998, *ApJ*, 505, 174
- González Delgado, R.M., Heckman, T., & Leitherer, C. 2001, *ApJ*, 546, 845
- González Delgado, R.M., Cid Fernandes, R., Pérez, E., Martins, L. P., Storchi-Bergmann, T., Schmitt, H., Heckman, T.M., & Leitherer, C. 2004, 605, 127
- González-Martín, O., Masegosa, J., Márquez, I., Guerrero, M.A., & Dultzin-Hacyan, D. 2006, *A&A*, 460, 45
- Graham, A.W., Erwin, P., Trujillo, I., & Asensio, R.A. 2003, *AJ*, 125, 2951
- Heckman, T. M. 1980, *A&A*, 87, 152
- Ho, L.C., Filippenko, A.V. & Sargent, W.L.W. 1995, *ApJ*, 98, 477
- Ho, L.C., Filippenko, A.V. & Sargent, W.L.W. 1997a, *ApJS*, 112, 315
- Ho, L.C., Filippenko, A.V. & Sargent, W.L.W. 1997b, *ApJS*, 112, 391
- Ho, L.C., Rudnick, G., Rix, H.-W., Shields, J.C., McIntosh, D.H., Filippenko, A.V., Sargent, W.L.W., & Eracleous, M. 2000, *ApJ*, 541, 120
- Holtzman, J.A., Burrows, C., Casertano, S., Hester, J., Trauger, J.T., Watson, A.M., Worthey, G. 1995, *PASP*, 107, 1065
- Hughes, M. A., Axon, D., Atkinson, J., Alonso-Herrero, A., Scarlata, C., Marconi, A., Batcheldor, D., Binney, J. 2005, *AJ*, 130, 73
- King, I.R. 1966, *AJ*, 71, 64
- Lauer, T.R., et al. 1995, *AJ*, 110, 2622
- Lauer, T.R., et al. 2005, *AJ*, 129, 2138
- Lauer, T.R., et al. 2006, (astro-ph/0609762)
- Maoz, D., Koratkar, A., Shields, J.C., Ho, L.C., Filippenko, A.V., & Sternberg, A. 1998, *AJ*, 116, 55
- Maoz, D., Nagar, N.M., Falcke, H., & Wilson, A.S. 2005, *ApJ*, 625, 699
- Martini, P., & Pogge, R.W. 1999, *AJ*, 118, 2646
- Martini, P., Regan, M.W., Mulchaey, J.S., Pogge, R.W. 2003, *ApJ*, 589, 774
- Meurer, G.R., Heckman, T.M., Leitherer, C., Kinney, A., Robert, C., & Garnett, D.R. 1995, *AJ*, 110, 2665
- Muñoz-Marín, V., González Delgado, R.M., Schmitt, H., et al. 2007, *AJ*, 134, 648
- Nagar, N.M., Falcke, H., Wilson, A.S., & Ho, L.C. 2000, *ApJ*, 542, 186

- Nagar, N.M., Falcke, H., Wilson, A.S., & Ulvestad, J.S. 2002, *A&A*, 392, 53
- Nagar, N. M., Falcke, E., & Wilson, A. S. 2005, *A&A*, 435, 521
- Pogge, R.W., & Martini, P. 2002, *ApJ*, 569, 624
- Ravindranath, S., Ho, L.C., Peng, C.Y., Filippenko, A.V., Sargent, W.L.W. 2001, *AJ*, 122, 653
- Regan, M.W., & Mulchaey, J.S. 1999, *AJ*, 117, 2676
- Rest, A., van den Bosch, F.C., Jaffe, W., Tran, H., Tsvetanov, Z., Ford, H.C., Davies, J., Schafer, J. 2001, *AJ*, 121, 2431
- Satyapal, S., Sambruna, R.M., & Dudik, R.P. 2004, *A&A*, 414, 825
- Scarlata, C., Stiavelli, M., Hughes, M. A., Axon, D., Alonso-Herrero, A., Atkinson, J., Batcheldor, D., Binney, J. et al. 2004, *AJ*, 128, 1124
- Schlegel, D.J., Finkbeiner, D.P., & Davis, M. 1998, *ApJ*, 500, 525
- Sérsic, J.-L. 1968, *Atlas de Galaxias Australes* (Córdoba: Obs. Astron., Univ. Nac. Córdoba)
- Shields, J.C., Rix, H.-W., McIntosh, D.H., Ho, L.C., Rudnick, G., Filippenko, A.V., Sargent, W.L.W., & Sarzi, M. 2000, *ApJ*, 534, L27
- Simoes Lopes, R.D., Storchi-Bergmann, T., de Fátima Saraiva, M., Martini, P. 2007, *ApJ*, 655, 718
- Storchi-Bergmann, T., Eracleous, M., Livio, M., Wilson, A.S., Filippenko, A.V., & Halpern, J.P. 1995, *ApJ*, 443, 617
- Taniguchi, Y., Shioya, Y., & Murayama, T. 2000, *AJ*, 120, 1265
- Terashima, Y., Ho, L.C., & Ptak, A.F. 2000, *ApJ*, 539, 161
- Tran, H.D., Tsvetanov, Z., Ford, H.C., Davies, J., Jaffe, W., van der Bosch, F.C., & Rest, A. 2001, *AJ*, 121, 2928
- Trujillo, I., Erwin, P., Asensio Ramos, A., & Graham, A.W. 2004, *AJ*, 127, 1917
- Tully, R.B., 1988, *Nearby Galaxies Catalog* (Cambridge: Cambridge Univ. Press)
- van der Marel, R. P., Rossa, J., Walcher, C. J., Boeker, T., Ho, L. C., Rix, H.-W., & Shields, J. C. 2007 in *Stellar Populations as Building Blocks of Galaxies*, eds. A. Vazdekis and R. Peletier (astro-ph/0702433)
- Verdoes Kleijn, G.A., & de Zeeuw, P.T. 2005, *A&A*, 387, 441

Table 1. Sample Properties

Galaxy Name	Spectral Class	Hubble Type	Type Type	vel. km s ⁻¹	dist. Mpc	pc/'' pc	[OI]/H α	W _K Å	Dn4000	SP Class
NGC266	L1.9	SB(rs)ab	2.0	4662	62.4	302	0.28	18.82	2.03	OL
NGC315	L1.9	E+	-4.0	4935	65.8	319	0.59	17.01	2.00	OL
NGC404	L2	SA(s)0-	-3.0	-46	2.4	11	0.17	9.82	1.50	YT
NGC428	L2/T2:	SAB(s)m	9.0	1160	14.9	72	0.19	14.83	1.65	YT
NGC660	T2/H:	SB(s)apec	1.0	852	11.8	57	0.047	14.53	1.72	YT
NGC841	L1.9:	(R')SAB(s)ab	2.1	4539	59.5	288	0.58	14.93	1.73	YL
NGC1161	T1.9:	SA0	-2.0	1940	25.9	125	0.14	18.98	2.16	OT
NGC2685	S2/T2:	(R)SB0+pec	-1.0	820	16.2	78	0.13	18.72	2.01	OT
NGC2787	L1.9	SB(r)0+	-1.0	691	13.0	63	0.55	16.82	2.08	OL
NGC2911	L2	SA(s)0:pec	-2.0	3183	42.2	204	0.31	17.72	2.05	OL
NGC3166	L2	SAB(rs)0/a	0.0	1344	22	106	0.27	15.88	1.80	OL
NGC3169	L2	SA(s)apec	1.0	1234	19.7	95	0.28	17.31	1.99	OL
NGC3226	L1.9	E2:pec	-5.0	1321	23.4	113	0.59	18.51	2.13	OL
NGC3245	T2:	SA(r)0?	-2.0	1348	22.2	107	0.086	15.21	1.79	OT
NGC3368	L2	SAB(rs)ab	2.0	897	8.1	39	0.18	10.12	1.48	YT
NGC3489	T2	SAB(rs)0+	-3.0	701	6.4	31	0.11	12.98	1.58	YT
NGC3507	L2	SB(s)b	3.0	978	19.8	96	0.18	5.44	1.26	YT
NGC3627	T2/S2	SAB(s)b	3.0	727	6.6	31	0.13	11.61	1.55	YT
NGC3675	T2	SA(s)b	3.0	766	12.8	9	0.12	18.45	2.17	OT
NGC3705	T2	SAB(r)ab	2.0	1018	17.0	82	0.079	14.8	1.73	YT
NGC3992	T2:	SB(rs)bc	4.0	1048	17.0	82	0.13	18.69	2.36	OT
NGC3998	L1.9	SA0	-2.0	1049	21.6	105	0.53	3.89	1.25	OL
NGC4143	L1.9	SAB(s)0	-2.0	783	17.0	82	0.71	14.85	1.72	OL
NGC4150	T2	SA(r)0?	-2.0	43	9.7	47	0.13	12.57	1.55	YT
NGC4192	T2	SAB(s)ab	2.0	-142	16.8	81	0.14	15.95	1.93	OT
NGC4203	L1.9	SAB0-	-3.0	1085	9.7	47	1.22	10.01	1.42	OL
NGC4261	L2	E2+	-5.0	2210	35.1	170	0.49	18.45	1.92	OL
NGC4314	L2	SB(rs)a	1.0	962	9.7	47	0.18	15.09	2.02	OT
NGC4321	T2	SAB(s)b	4.0	1234	16.8	81	0.11	7.49	1.32	YT
NGC4429	T2	SA(r)0+	-1.0	1137	16.8	81	0.097	15.79	1.95	OT
NGC4435	T2	SB(s)0	-2.0	781	16.8	81	0.13	15.06	1.96	OT
NGC4438	L1.9	SA(s)0/a:	0.0	64	16.8	81	0.27	17.85	2.00	OL
NGC4450	L1.9	SA(s)ab	2.0	1956	16.8	81	0.67	11.74	1.52	OL
NGC4459	T2	SA(r)0+	-1.0	1202	16.8	81	0.13	14.83	2.21	YT
NGC4569	T2	SAB(rs)ab	0.0	-235	16.8	81	0.062	4.99	1.21	YT
NGC4596	L2::	SB(r)0+	-1.0	1874	16.8	81	0.27	15.9	2.05	OL
NGC4736	L2	(R)SA(r)ab	2.0	307	4.3	20	0.24	12.93	1.67	YT
NGC4826	T2	(R)SA(rs)ab	2.0	411	4.1	19	0.073	14.43	1.76	YT
NGC5005	L1.9	SAB(rs)bc	4.0	948	21.3	103	0.65	14.6	1.74	YL
NGC5055	T2	SA(rs)bc	4.0	504	7.2	34	0.17	14.07	1.75	YT
NGC5377	L2	(R)SB(s)a	1.0	1792	31.0	150	0.25	8.66	1.45	YT
NGC5678	T2	SAB(rs)b	3.0	1924	35.6	172	0.079	8.7	1.48	YT
NGC5879	T2/L2	SA(rs)bc?	4.0	772	16.8	81	0.16	16.3	1.72	OT
NGC5970	L2/T2:	SB(r)c	5.0	1965	31.6	153	0.18	18.39	1.86	OT
NGC5982	L2::	E3	-5.0	2904	38.7	187	0.49	18.11	2.05	OL
NGC5985	L2	SAB(r)b	3.0	2518	39.2	190	0.30	18.9	1.97	OL
NGC6340	L2	SA(s)0/a	0.0	1207	22.0	106	0.43	20.04	2.26	OL
NGC6384	T2	SAB(r)bc	4.0	1667	26.6	128	0.15	18.6	1.92	OT
NGC6500	L2	SAab:	1.7	2999	39.7	192	0.23	15.81	1.74	OT
NGC6503	T2/S2:	SA(s)cd	6.0	42	6.1	29	0.08	9.49	1.36	YT
NGC6703	L2::	SA0-	-2.5	2364	35.9	174	0.36	18.53	2.11	OL
NGC6951	S2	SAB(rs)bc	4.0	1424	24.1	116	0.23	16.4	1.70	OT
NGC7177	T2	SAB(r)b	3.0	1147	18.2	88	0.14	16.64	1.80	OT
NGC7217	L2	(R)SA(r)ab	2.0	945	16.0	77	0.25	19.2	2.07	OT
NGC7331	T2	SA(s)b	3.0	821	14.3	69	0.097	18.03	1.99	OT
NGC7626	L2::	E:pec	-5.0	3422	45.6	221	0.22	18.08	2.12	OT
NGC7742	T2/L2	SA(r)b	3.0	1653	22.2	107	0.13	17.07	1.90	OT

Note. — Col. (1): Galaxy name; Col. (2): Spectral class. Col. (3): Hubble type. Col. (4): Numerical Hubble type. Col. (5): Radial velocity. Col. (6): Distance. Col. (7): Angular scale. Col. (8): [OI]/H α flux ratio. All these quantities were extracted from HFS97. Col. (9): Equivalent width of CaII K line. Col. (10): The 4000 Å break. Col. (11): Stellar population class. O: old, Y: young population. These three columns are from Cid Fernandes et al. (2004) and González Delgado et al. (2004).

^{1,2}Grouped among TOs in this paper.

³Grouped with LINERs in this paper (see Pérez et al. 2000).

Table 2. Observations

Galaxy Name	Filter	Texps	scale arcsec/pix	orient deg	ID	Filter	Texps	scale arcsec/pix	orient deg	ID
NGC 266	F547M	360	0.0456	-56.5	6837					
NGC 315	F547M	360	0.0456	-55.7	6837	F814W	460.0	0.0456	97.10	6673
	F555W	460	0.0456	97.1	6673					
NGC 404	F547M	350	0.0456	-156.0	6871	F814W	320.0	0.0456	-92.90	5999
	F555W	160	0.0456	-92.9	5999					
NGC 428	F606W	460	0.100	-157.7	9042	F814W	640.0	0.0456	112.0	8599
NGC 660	F606W	160	0.100	-155.1	5446	F814W	460.0	0.100	-154.9	9042
NGC 841	F547M	400	0.0456	117.0	6837					
NGC 1161	F547M	360	0.0456	-113.0	6837					
NGC 2685	F555W	1000	0.0456	-135.0	6633	F814W	730.0	0.0456	-135.0	6633
NGC 2787	F547M	360	0.0456	26.8	6837	F814W	730.0	0.0456	-125.0	6633
	F555W	1000	0.0456	-125.0	6633					
NGC 2911	F547M	460	0.100	-115.6	5924					
NGC 3166	F547M	300	0.0456	-29.0	5419					
NGC 3169	F547M	260	0.0456	-25.9	5419	F814W	460.0	0.100	-115.8	9042
NGC 3226	F547M	460	0.0456	173.0	6837					
NGC 3245	F547M	360	0.0456	178.0	6837					
NGC 3368	F606W	320	0.100	-110.8	9042	F814W	320.0	0.100	-110.8	9042
NGC 3489	F555W	100	0.0456	-31.7	5999	F814W	200.0	0.0456	-31.70	5999
NGC 3507	F606W	160	0.0456	151.0	5446					
NGC 3627	F606W	560	0.0456	-20.1	8597					
NGC 3675	F606W	160	0.100	-119.4	5446					
NGC 3705	F606W	160	0.100	64.3	5446	F814W	460.0	0.100	-107.6	9042
NGC 3992	F547M	230	0.0456	149.0	5419					
NGC 3998	F547M	240	0.0456	-128.0	5924	F791W	100.0	0.0456	-128.0	5924
NGC 4143	F606W	560	0.0456	-77.2	8597					
NGC 4150	F555W	160	0.0456	-40.4	5999	F814W	320.0	0.0456	-40.40	5999
NGC 4192	F547M	720	0.0456	149.0	6436	F814W	660.0	0.0456	167.0	5375
	F555W	660	0.0456	167.0	5375	F791W	720.0	0.0456	149.0	6436
NGC 4203	F547M	300	0.0456	11.9	5419	F814W	320.0	0.0456	-12.20	5999
	F555W	160	0.0456	-12.2	5999					
NGC 4261	F547M	800	0.0456	-20.3	5124	F791W	800.0	0.0456	-20.30	5124
NGC 4314	F606W	560	0.0456	-10.7	8597	F814W	600.0	0.0456	-5.310	6265
NGC 4321	F555W	1668	0.0456	-26.1	5195					
NGC 4429	F606W	160	0.0456	151.0	5446					
NGC 4435						F814W	520.0	0.0456	-93.40	6791
NGC 4438						F814W	1050	0.100	-169.7	6791
NGC 4450	F555W	460	0.0456	175.0	5375	F814W	460.0	0.0456	175.0	5375
NGC 4459	F555W	160	0.0456	-111.0	5999	F814W	320.0	0.0456	-111.0	5999
NGC 4569	F547M	126	0.0456	-164.0	6436	F791W	126.00	0.0456	-164.0	6436
NGC 4596	F606W	160	0.0456	153.0	5446					
NGC 4736	F555W	296	0.0456	23.3	5741					
NGC 4826	F547M	1600	0.0456	-140.0	8591					
NGC 5005	F547M	230	0.0456	161.0	5419	F791W	120.0	0.0456	-168.0	6436
	F606W	560	0.0456	167.0	8597	F791W	600.0	0.0456	-168.0	6436
NGC 5055	F606W	160	0.0456	161.0	5446	F814W	460.0	0.100	-78.09	9042
	F547M	1050	0.0456	-0.04	8591					
NGC 5377	F606W	600	0.0456	-156.0	6359					
NGC 5678	F606W	600	0.0456	-103.0	6359					
NGC 5879	F606W	600	0.0456	157.0	6359	F814W	170.0	0.0456	77.20	7450
NGC 5970	F606W	560	0.0456	179.0	8597					
NGC 5982	F555W	1000	0.0456	-134.0	5454	F814W	460.0	0.0456	-134.0	5454
NGC 5985	F606W	600	0.0456	-68.4	6359					
NGC 6340	F606W	600	0.0456	-129.0	6359					
NGC 6384	F606W	600	0.0456	-83.3	6359					
NGC 6500	F547M	350	0.0456	-12.2	5419					
NGC 6503	F606W	160	0.0456	-178.0	5446					
NGC 6703	F555W	160	0.0456	68.1	5999	F814W	320.0	0.0456	68.10	5999
NGC 6951	F606W	560	0.0456	114.0	8597	F814W	700.0	0.100	43.16	8602
	F547M	300	0.0456	-123.0	5419					
NGC 7177	F606W	560	0.0456	136.0	8597	F814W	460.0	0.100	-176.7	9042
NGC 7217	F547M	300	0.0456	-73.0	5419	F814W	460.0	0.100	-178.0	9042
	F547M	300	0.0456	-73.0	5419					
NGC 7331						F814W	170.0	0.0456	-115.0	7450
NGC 7626	F555W	1000	0.0456	-65.5	5454	F814W	460.0	0.0456	-65.50	5454
NGC 7742	F555W	480	0.100	-163.1	6276	F814W	680.0	0.100	-163.1	6276

Table 2—Continued

Galaxy Name	Filter	Texps	scale arcsec/pix	orient deg	ID	Filter	Texps	scale arcsec/pix	orient deg	ID
-------------	--------	-------	------------------	------------	----	--------	-------	------------------	------------	----

Table 3. Dust and nuclear morphology

Galaxy Name	dust morph	dust distr	nucleated	Comments
NGC 266	LW	inout	Y	Spiral dust lanes, a small nuclear dust disk?
NGC 315	D	in	Y	Nuclear dust disk and dust chaotic filaments, a nuclear compact source
NGC 404	CS	in	Y	Nuclear stellar cluster, spiral and chaotic filaments
NGC 428	N	–	Y	Two nuclear stellar clusters, the brightest one at the center of the galaxy
NGC 660	LW	inout	no	Spiral dust lane structure, the position of the center is not clear
NGC 841	GD	inout	C+D	A spiral dust lane down to the center, several central sources?
NGC 1161	TW	inout	no?	Well organized spiral dust lanes, an extended nucleus ?
NGC 2685	C	inout	no?	Chaotic dust morphology at the NE, a strong nuclear stellar disk
NGC 2787	TW	inout	Y	Dust ring perpendicular to the galaxy major axis, a nuclear central source
NGC 2911	C	inout	no	Highly obscured center with chaotic filaments
NGC 3166	CS	inout	no	Very perturbed central morphology, chaotic dust lanes down the center
NGC 3169	CS	inout	no	Chaotic spiral dust lanes down to the center
NGC 3226	D	in	Y	Dust disk and a nuclear source
NGC 3245	D	in	Y	Dust disk and a nuclear source
NGC 3368	CS	inout	Y?	Perturbed center, with chaotic spiral dust lanes, a compact nuclear source
NGC 3489	CS	in	Y	Chaotic spiral dust lanes down the center, a stellar disk and/or a nuclear compact source
NGC 3507	C	in	Y	Some chaotic dust filaments, a nuclear stellar cluster
NGC 3627	C	inout	C+D	Chaotic dust lanes, several sources at the center
NGC 3675	TW	inout	no	Spiral dust lanes out to large distance
NGC 3705	GD	inout	no?	Spiral dust lanes toward the center, maybe with a stellar disk or an extended nuclear source
NGC 3992	C	in	no	Only a few dust filaments around, light profile follows a $r^{1/4}$
NGC 3998	N	–	Y	Almost no dust around, a bright nuclear compact source
NGC 4143	LW	inout	no?	Weak coherent spiral dust lanes, maybe a weak nuclear compact source
NGC 4150	C	in	no	Highly perturbed center, chaotic dust lanes across the nucleus
NGC 4192	CS	inout	C+D	Highly inclined galaxy, chaotic dust and one or several compact sources not at the center
NGC 4203	TW	in	Y	Some weak spiral dust lane around a bright nuclear compact source
NGC 4261	D	in	Y	Nuclear dust disk, and a weak nuclear compact source
NGC 4314	LW	inout	no	Star formation ring, spiral dust lanes associated to the ring
NGC 4321	LW	inout	Y	Star formation in arms spiraling toward the nucleus with dust lanes associated, a compact nuclear cluster
NGC 4429	LW	inout	Y	Well structured spiral ring, a compact source and/or a small stellar disk
NGC 4435	D	in	no	High inclined dust disk
NGC 4438	C	inout	no	Very perturbed central morphology, chaotic dust lanes across the center
NGC 4450	C	inout	Y	Chaotic dust lanes, a bright nuclear compact source
NGC 4459	TW	inout	Y?	Dust spiral ring, a nuclear source
NGC 4569	C	inout	Y	Chaotic dust lanes, a nuclear stellar cluster
NGC 4596	N	out	Y	Very faint dust spiral structure, a nuclear compact source
NGC 4736	TW	inout	Y	Spiral dust lanes down the nucleus, a compact nuclear stellar cluster
NGC 4826	TW	in	no	Inner spiral arms with star formation, dust associated to the arms
NGC 5005	CS	inout	D+C	Chaotic nuclear spirals, center is obscured but several central knots are visible
NGC 5055	C	in	Y	Dust is mainly in the S part, probably an extended nuclear source
NGC 5377	TW	inout	Y?	Spiral dust lanes toward the nucleus, an extended nuclear source
NGC 5678	CS	inout	Y	Chaotic dust lanes toward the center, a nuclear source
NGC 5879	LW	inout	Y	Weak nuclear source
NGC 5970	LW	inout	Y	Spiral dust lanes, a faint compact nuclear source
NGC 5982	N	–	no	No dust, a core light distribution
NGC 5985	C	inout	Y?	A faint nuclear stellar cluster
NGC 6340	N	–	no	Light profile follows a $r^{1/4}$
NGC 6384	CS	inout	Y	Dust lane toward the nucleus, a faint nuclear stellar cluster
NGC 6500	C	inout	no	Several nuclear sources?
NGC 6503	CS	in	C	A nuclear bar structure, several central sources?
NGC 6703	N	–	no?	No dust
NGC 6951	LW	inout	no?	A star forming ring, dust associated to the ring with spiral lanes toward the center, several nuclear sources?
NGC 7177	C	inout	no	Very perturbed morphology, chaotic dust through the nucleus
NGC 7217	LW	inout	no	Coherent spiral dust structure, small dust lane through the nucleus
NGC 7331	C	inout	Y?	Chaotic dust lanes, a nuclear source?
NGC 7626	N?	–	no	Core light profile. Only a tiny dust disk or dust lane through the nucleus
NGC 7742	LW	out	Y?	Star forming ring, dust lanes associated to the ring, maybe a compact nucleus

Table 4. Frequency of Dust Morphologies

Dust morphology	LLAGNs	strong-[OI]	weak-[OI]	Seyferts	Late LLAGNs	Early LLAGNs	Early type galaxies	Early type (e.l.)
No dust (N)	12%	25%	5%	3%	3%	24%	45%	10%
Dust disk (D)	9%	15%	5%	0%	0%	20%	22%	31%
Chaotic dust (C+CS)	42%	35%	46%	30%	50%	32%	17%+7%	35%
Spiral dust (GD+TW+LW)	37%	25%	43%	67%	47%	24%	9%	14%

Note. — Col. (2-4): this work for LLAGNs, strong-[OI], and weak-[OI] LLAGNs, respectively. Col. (5): Seyfert galaxies from Martini et al. (2003). Col. (6-7): this work for early and late type LLAGN hosts, respectively. Col. (8 and 9): Early type galaxies and early type galaxies with emission lines from Laier et al. (2005).

Table 5. Total central magnitudes and surface brightness at 0.2, 0.5 and 1 arcsec

Galaxy Name	Filter	E(B-V)	mag02 mag	mag05 mag	mag1 mag	μ 02 mag/arcsec ²	μ 05 mag/arcsec ²	μ 1 mag/arcsec ²
NGC 266	F547m	0.069	18.43	16.73	15.60	16.28	16.69	17.20
NGC 315	F547m	0.065	19.52	17.48	15.97	17.31	17.19	17.28
NGC 315	F555w	0.065	19.36	17.42	15.94	17.24	17.15	17.25
NGC 404	F547m	0.059	15.91	15.16	14.58	14.42	15.99	16.72
NGC 404	F555w	0.059	15.92	15.15	14.55	14.37	15.94	16.67
NGC 841	F547m	0.048	18.03	16.23	15.07	15.78	16.14	16.79
NGC 1161	F547m	0.22	16.97	15.46	14.61	14.72	15.69	16.46
NGC 2685	F555w	0.062	17.59	16.03	15.00	15.41	16.11	16.69
NGC 2787	F547m	0.13	16.84	15.43	14.50	14.73	15.63	16.34
NGC 2787	F555w	0.13	16.81	15.41	14.48	14.70	15.61	16.31
NGC 2911	F547m	0.031	18.23	16.89	15.97	16.07	17.11	17.62
NGC 3166	F547m	0.031	17.87	15.84	14.68	15.45	15.74	16.30
NGC 3169	F547m	0.031	17.54	16.03	15.14	15.29	16.10	16.95
NGC 3226	F547m	0.023	17.22	15.95	15.26	15.12	16.31	17.47
NGC 3245	F547m	0.025	17.07	15.60	14.60	14.93	15.76	16.24
NGC 3489	F555w	0.017	15.47	14.27	13.50	13.47	14.63	15.53
NGC 3992	F547m	0.029	17.79	16.29	15.37	15.59	16.46	17.17
NGC 3998	F547m	0.016	15.93	14.77	13.91	14.11	15.10	15.73
NGC 4150	F555w	0.018	19.25	16.46	15.09	16.69	16.05	16.58
NGC 4192	F547m	0.035	17.63	16.26	15.39	15.38	16.62	17.11
NGC 4192	F555w	0.035	17.63	16.25	15.38	15.37	16.59	17.11
NGC 4203	F547m	0.012	16.94	15.52	14.53	14.87	15.66	16.22
NGC 4203	F555w	0.012	16.82	15.45	14.49	14.84	15.64	16.21
NGC 4261	F547m	0.018	19.13	16.94	15.32	16.73	16.59	16.54
NGC 4321	F555w	0.026	17.71	16.62	15.76	15.83	16.98	17.56
NGC 4450	F555w	0.028	17.09	15.70	14.81	15.01	15.94	16.66
NGC 4459	F555w	0.046	16.62	15.16	14.29	14.49	15.35	16.15
NGC 4569	F547m	0.046	14.43	13.76	13.29	12.85	14.65	15.78
NGC 4736	F555w	0.018	15.53	14.11	13.17	13.39	14.33	14.96
NGC 4826	F547m	0.041	16.50	14.94	14.00	14.23	15.09	15.84
NGC 5005	F547m	0.014	17.30	15.51	14.40	14.94	15.46	16.06
NGC 5055	F547m	0.018	15.70	14.59	14.00	13.71	15.10	16.45
NGC 5982	F555w	0.018	17.80	15.89	14.81	15.39	15.86	16.51
NGC 6500	F547m	0.090	17.97	16.32	15.36	15.60	16.45	17.18
NGC 6703	F555w	0.089	16.73	15.45	14.67	14.61	15.81	16.63
NGC 6951	F547m	0.37	17.36	16.07	15.12	15.25	16.38	16.76
NGC 7217	F547m	0.088	18.05	16.14	14.98	15.71	16.06	16.60
NGC 7626	F555w	0.072	18.16	16.27	15.21	15.75	16.26	16.91
NGC 7742	F555w	0.055	16.88	15.65	14.91	14.75	15.93	16.92
NGC 428	F606w	0.028	19.35	18.71	18.04	17.42	19.55	19.97
NGC 660	F606w	0.065	20.09	18.27	16.93	17.87	18.09	18.29
NGC 3368	F606w	0.025	16.95	15.51	14.52	14.75	15.63	16.20
NGC 3507	F606w	0.024	17.46	16.51	15.75	15.53	17.05	17.62
NGC 3627	F606w	0.032	17.60	15.75	14.59	15.23	15.76	16.08
NGC 3675	F606w	0.020	17.17	15.77	14.93	15.00	15.95	16.84
NGC 3705	F606w	0.046	17.63	16.21	15.46	15.48	16.34	17.55
NGC 4143	F606w	0.013	16.97	15.38	14.39	14.76	15.48	16.13
NGC 4314	F606w	0.025	17.95	16.35	15.34	15.72	16.43	17.03
NGC 4429	F606w	0.033	17.24	15.94	15.07	15.14	16.28	16.84
NGC 4596	F606w	0.022	17.53	16.13	15.15	15.48	16.29	16.82
NGC 5005	F606w	0.014	17.19	15.36	14.26	14.81	15.27	15.92
NGC 5055	F606w	0.018	15.54	14.49	13.91	13.56	15.05	16.33
NGC 5377	F606w	0.016	17.01	16.00	15.28	14.88	16.65	17.17
NGC 5678	F606w	0.011	18.63	17.36	16.41	16.58	17.61	18.04
NGC 5879	F606w	0.012	18.95	17.33	16.18	16.76	17.38	17.67
NGC 5970	F606w	0.042	19.71	17.89	16.60	17.47	17.78	18.05
NGC 5985	F606w	0.017	18.99	17.56	16.61	16.83	17.75	18.31
NGC 6340	F606w	0.049	17.46	15.92	15.05	15.25	16.14	16.94
NGC 6384	F606w	0.12	18.70	16.92	15.72	16.51	16.84	17.25
NGC 6503	F606w	0.032	18.71	17.43	16.51	16.69	17.63	18.29
NGC 6951	F606w	0.37	17.26	15.94	15.02	15.10	16.24	16.68
NGC 7177	F606w	0.072	18.86	17.03	15.82	16.47	17.00	17.25
NGC 315	F814w	0.065	19.12	17.27	15.83	17.03	17.03	17.18
NGC 404	F814w	0.059	16.19	15.41	14.79	14.46	16.17	16.90
NGC 428	F814w	0.028	19.52	18.97	18.31	18.05	19.88	20.27
NGC 660	F814w	0.065	19.67	17.79	16.38	17.45	17.59	17.69

Table 5—Continued

Galaxy Name	Filter	E(B-V)	mag02 mag	mag05 mag	mag1 mag	μ 02 mag/arcsec ²	μ 05 mag/arcsec ²	μ 1 mag/arcsec ²
NGC 2685	F814w	0.062	17.46	15.98	15.00	15.29	16.13	16.72
NGC 2787	F814w	0.13	16.80	15.37	14.44	14.63	15.57	16.23
NGC 3169	F814w	0.031	17.13	15.62	14.70	14.94	15.69	16.48
NGC 3368	F814w	0.025	16.85	15.46	14.46	14.68	15.59	16.12
NGC 3489	F814w	0.017	15.80	14.52	13.70	13.71	14.83	15.63
NGC 3705	F814w	0.046	17.55	16.10	15.35	15.39	16.23	17.47
NGC 3998	F791w	0.016	15.93	14.71	13.85	13.97	15.02	15.67
NGC 4150	F814w	0.018	18.48	16.20	15.05	15.99	16.04	16.70
NGC 4192	F791w	0.035	17.25	15.82	14.93	15.01	16.10	16.68
NGC 4192	F814w	0.035	17.24	15.81	14.92	15.00	16.10	16.66
NGC 4203	F814w	0.012	16.85	15.40	14.41	14.72	15.54	16.14
NGC 4261	F791w	0.018	18.90	16.71	15.19	16.49	16.42	16.47
NGC 4314	F814w	0.025	17.93	16.32	15.31	15.68	16.41	17.02
NGC 4435	F814w	0.030	17.69	16.00	14.93	15.37	16.04	16.53
NGC 4438	F814w	0.028	17.48	15.91	14.94	15.27	15.99	16.65
NGC 4450	F814w	0.028	17.10	15.69	14.81	14.95	15.92	16.65
NGC 4459	F814w	0.046	16.58	15.09	14.23	14.39	15.28	16.14
NGC 4569	F791w	0.046	15.06	14.25	13.68	13.25	14.98	15.94
NGC 5005	F791w	0.014	17.27	15.27	14.17	14.86	15.11	15.81
NGC 5055	F814w	0.018	17.00	15.13	14.15	14.78	14.98	16.08
NGC 5879	F814w	0.012	18.88	17.25	16.12	16.68	17.28	17.64
NGC 5982	F814w	0.018	17.82	15.91	14.83	15.41	15.87	16.52
NGC 6703	F814w	0.089	16.73	15.45	14.67	14.57	15.82	16.63
NGC 6951	F814w	0.37	17.41	16.05	15.06	15.25	16.21	16.68
NGC 7177	F814w	0.072	18.63	16.91	15.69	16.41	16.83	17.11
NGC 7217	F814w	0.088	17.71	16.00	14.88	15.52	15.91	16.50
NGC 7331	F814w	0.091	16.14	14.75	13.88	13.97	15.03	15.71
NGC 7626	F814w	0.072	18.03	16.20	15.16	15.65	16.21	16.87
NGC 7742	F814w	0.055	17.14	15.80	15.03	14.96	16.03	17.00

Note. — STSMAG magnitudes (in the F547M, F555W, F606W, and F814W or F791W) calculated integrating the total flux in a circular aperture of 0.2, 0.5 and 1 arcsec radius (columns 4, 5, and 6, respectively). The surface brightness is calculated at 0.2, 0.5 and 1 arcsec distance from the center (columns 7, 8 and 9, respectively).

Table 6. Mean values of the central magnitude and surface brightness

	mag02	mag05	mag1	μ 02	μ 05	μ 1	in/out slope
All in V	17.6	16.1	15.1	15.5	16.3	16.9	2.3
TO	17.6	16.1	15.2	15.5	16.4	17.0	2.5
LINERs	17.6	16.1	15.0	15.5	16.1	16.8	2.1
Young SP	17.2	15.9	14.9	15.1	16.1	16.8	2.2
Old SP	17.9	16.3	15.3	15.7	16.4	17.0	2.1
All in I	17.4	15.9	15.1	15.2	16.0	16.6	2.0
TO	17.5	16.0	15.1	15.3	16.2	16.8	2.1
LINERs	17.4	15.8	14.7	15.2	15.8	16.4	1.8
Young SP	17.2	15.7	14.8	15.1	15.9	16.7	2.2
Old SP	17.7	16.1	15.0	15.4	16.1	16.7	1.9

Note. — Magnitudes are tabulated for the central 0.2, 0.5 and 1 arcsec radius (columns 2, 3 and 4), and the surface brightness at 0.2, 0.5 and 1 arcsec distance from the center (columns 5, 6, and 7).

Table 7. Frequency of compact nuclear sources in LLAGNs

	LLAGNs (57)	strong-[OI] (20)	weak-[OI] (37)	YTO (18)	OT (19)	YL (2)	OL (18)
No-nucleated	40%	40%	41 %	22%	58%	0%	44%
Nucleated	51%	50%	51 %	67%	37%	0%	55%
Clusters+dust?	9%	10%	8 %	11%	5%	100%	0%

Note. — The numbers in brackets indicate the number of objects of each type

Table 8. Nuclear magnitudes of the nucleated LLAGNs

Galaxy Name	Filter	radius	mag	mag	mag	mag	mag	μ (mag/arcsec ²)	F(15 GHz) (mJy)
NGC 266	F547m	0.14	19.72	19.59	20.08	19.63	19.84	16.65	4.1
NGC 315	F555w	0.14	20.70	20.64	20.96	20.73	20.73	17.62	470.0
NGC 404	F555w	0.23	16.03	15.98	16.12	15.98	16.11	14.06	<1.3
NGC 428	F606w	0.40	19.16	19.14	19.23	19.13	19.18	18.41	<0.9
NGC 2787	F555w	0.23	17.25	17.16	17.42	17.15	17.39	15.28	7.0
NGC 3226	F547m	0.23	17.53	17.44	17.71	17.43	17.68	15.56	5.4
NGC 3245	F547m	0.23	17.61	17.51	17.77	17.50	17.76	15.64	<1.0
NGC 3368	F606w	0.50	16.31	16.23	16.47	16.21	16.44	16.05	<1.0
NGC 3489	F555w	0.23	15.75	15.68	15.90	15.67	15.87	13.79	<1.0
NGC 3507	F606w	0.18	17.79	17.68	18.04	17.72	17.91	15.33	<1.5
NGC 3998	F547m	0.18	16.39	16.31	16.55	16.33	16.49	13.94	57.0
NGC 4203	F555w	0.18	17.48	17.39	17.66	17.41	17.58	15.03	9.0
NGC 4261	F547m	0.14	22.32	22.22	22.52	22.35	22.36	19.24	300.0
NGC 4321	F555w	0.23	17.91	17.84	18.05	17.86	18.01	15.95	<0.9
NGC 4429	F606w	0.18	17.87	17.73	18.13	17.75	18.05	15.42	<1.1
NGC 4450	F555w	0.18	17.80	17.68	18.02	17.69	17.96	15.35	2.7
NGC 4459	F555w	0.18	17.40	17.26	17.64	17.29	17.57	14.95	<1.0
NGC 4569	F547m	0.23	14.49	14.45	14.59	14.46	14.56	12.53	<1.1
NGC 4596	F606w	0.23	17.97	17.89	18.11	17.89	18.08	16.00	<1.1
NGC 4736	F555w	0.18	16.28	16.14	16.54	16.17	16.46	13.83	1.7
NGC 5055	F547m	0.27	15.74	15.67	15.84	15.66	15.86	14.17	<1.1
NGC 5377	F606w	0.32	16.75	16.72	16.83	16.71	16.82	15.52	3.1
NGC 5678	F606w	0.18	19.21	19.08	19.45	19.10	19.37	16.75	<1.0
NGC 5879	F606w	0.18	19.94	19.83	20.19	19.84	20.08	17.49	<1.1
NGC 5970	F606w	0.18	21.08	20.99	21.27	20.97	21.19	18.63	...
NGC 5985	F606w	0.18	19.73	19.59	20.02	19.61	19.90	17.28	...
NGC 6384	F606w	0.18	19.94	19.86	20.12	19.85	20.02	17.49	<1.0
NGC 7742	F555w	0.50	16.12	16.03	16.28	16.03	16.25	15.85	<1.1

Note. — Column (3): number of arcsec used as radius (r_{in}) to measure the nuclear magnitude. Column (4-6): nuclear magnitudes measured within r_{in} , $r_{in}+1$ pixel, $r_{in}-1$ pixel and subtracted of the underlying galaxy contribution assuming that the underlying galaxy have central constant surface brightness that is equal to the value measured in an annulus with inner and outer radii of $r_{in}+1$ and $r_{in}+3$. Column (7-8): as in column 4 but now the surface brightness of the underlying light contribution is calculated at the annulus with inner and outer radii of $r_{in}+2$ and $r_{in}+4$ (column 7) and inner and outer radii of r_{in} and $r_{in}+2$ (column 8). Column (9): nuclear surface brightness estimated using columns (3) and (4). Column (10): Nuclear radio 15 GHz fluxes from Nagar et al. (2005), upper limits correspond to 5σ .

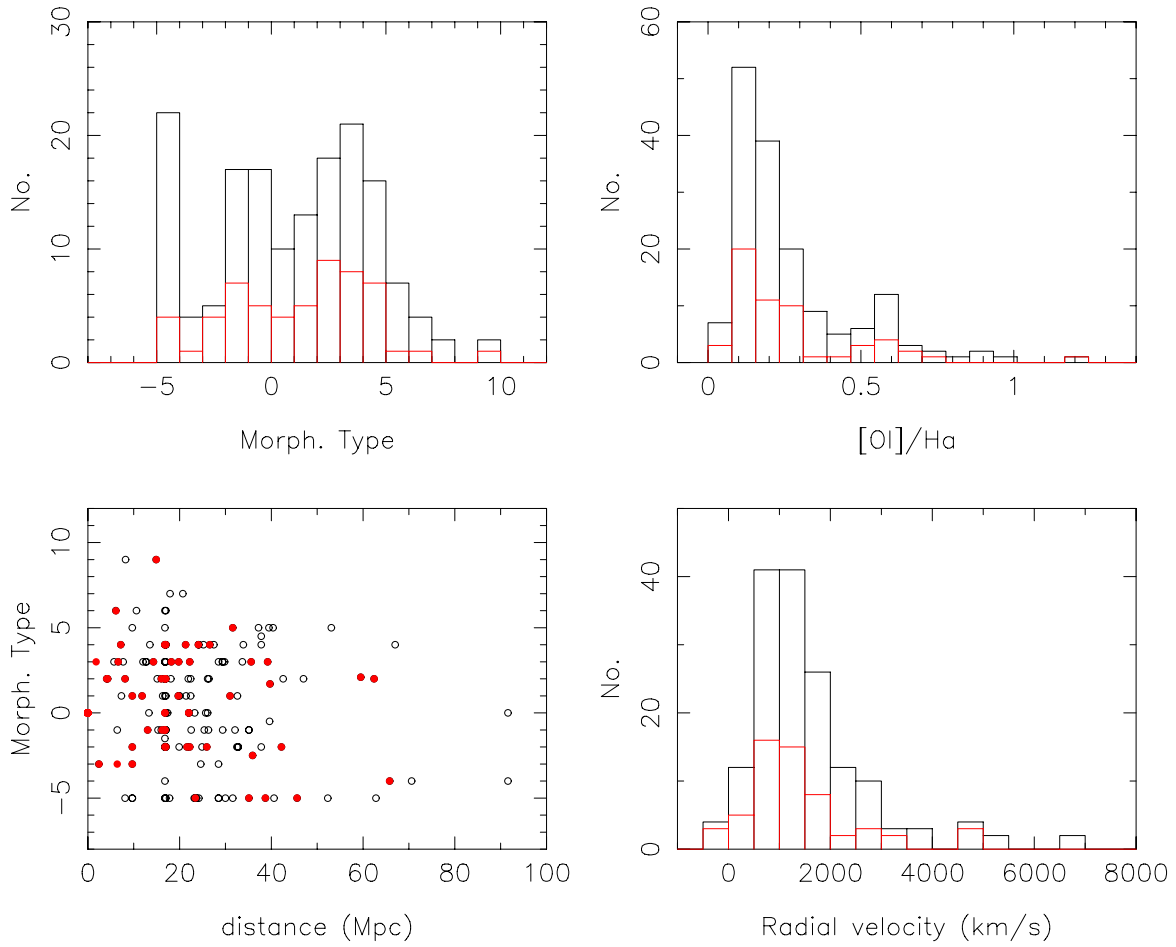


Fig. 1.— Distances and morphological T types for LLAGN in the HFS97 sample. Filled symbols and red lines in the histograms indicate objects in our sample. (All data extracted from HFS97.)

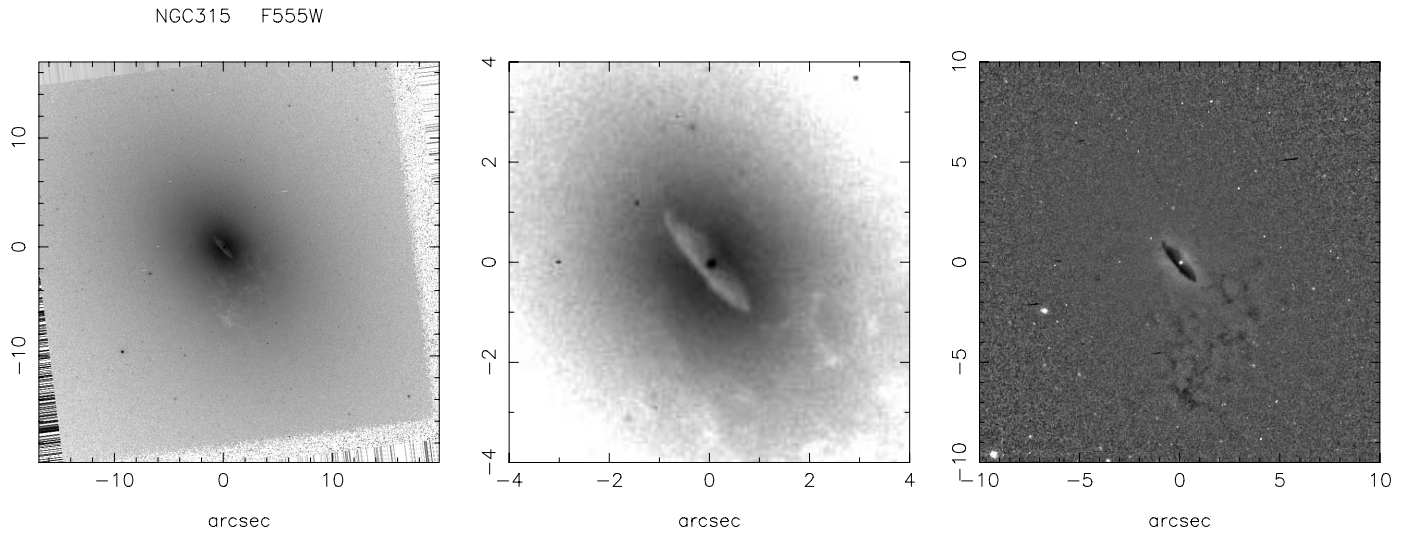


Fig. 2.— Atlas of the HST+WFPC2 images of the sample galaxies at three scales, (left:) the full PC frame (or the central ± 50 arcsec of the WFPC2 when the center is not in the PC chip; (center:) a zoom into the central ± 4 arcsec; (right:) the central ± 10 arcsec of the median filtered contrast image.

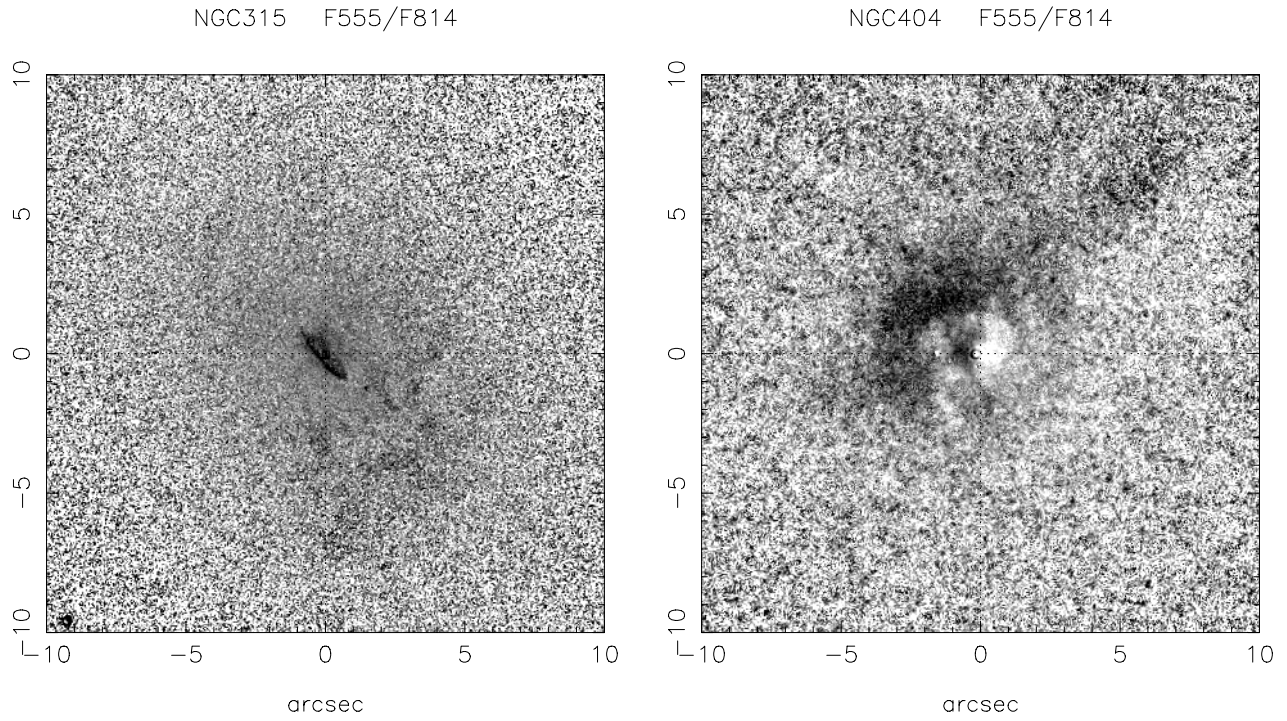


Fig. 3.— Color images of the galaxies observed in V and I filters. The dotted lines indicate the image center. Two sets of this color figures are produced according to the V filter available: (a) F555W/F814W, and (b) F606W/F814W.

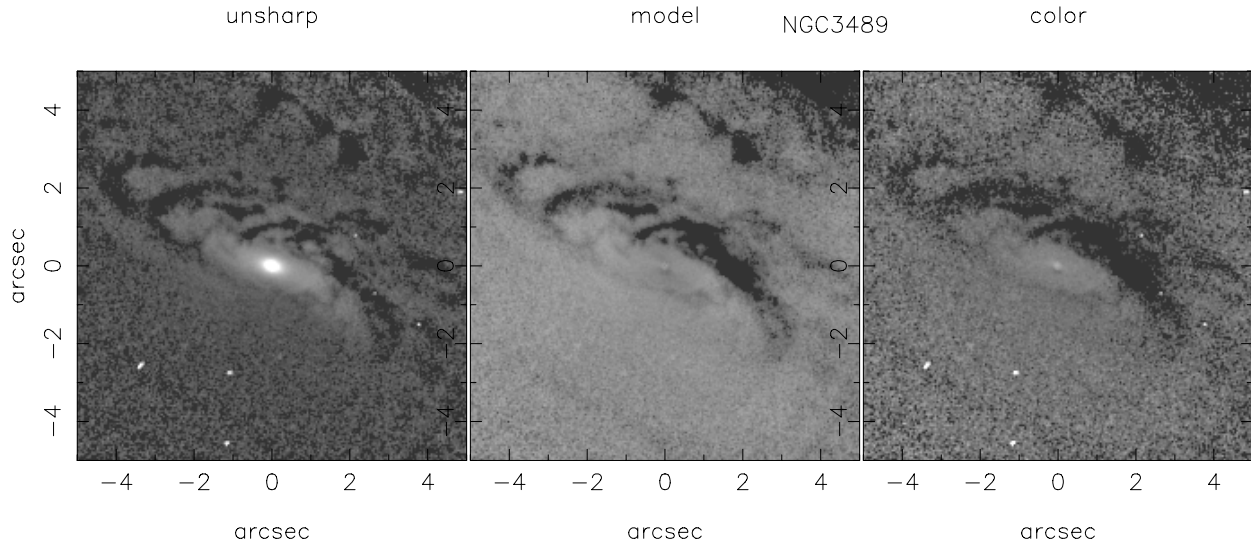


Fig. 4.— Three images of NGC 3489; (left:) un-sharp image; (center:) original image divided by the isophotal model image model; (right:) color image obtained dividing the F555W image by the F814W image.

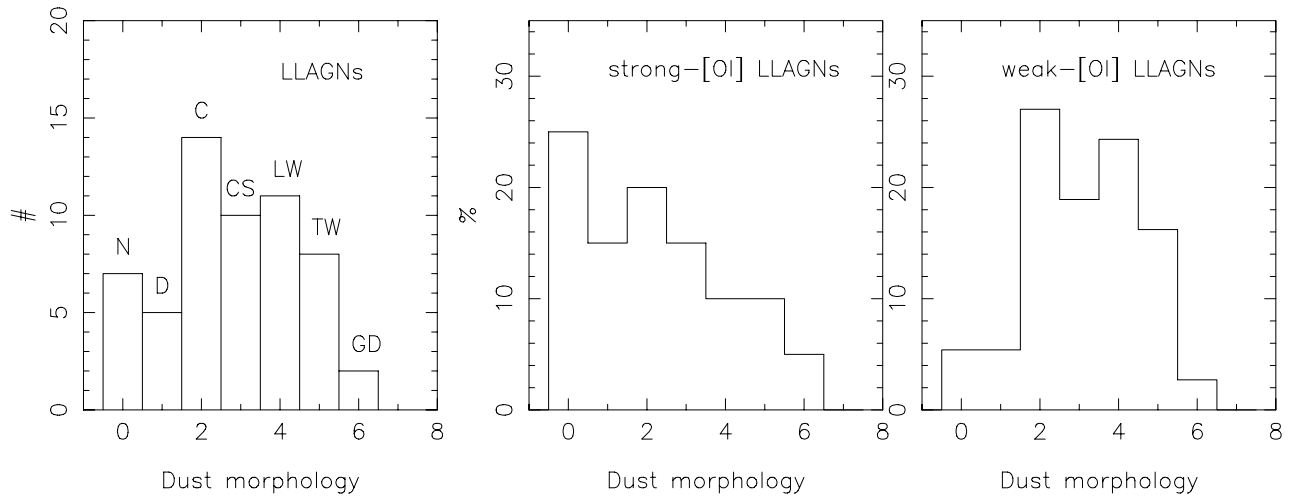


Fig. 5.— Histogram of the dust morphology distribution: (a), strong-[OI] (b) and weak-[OI] LLAGNs (c), into the seven classes defined: (0) No dust (N). (1) Disk dust (D). (2) Chaotic circumnuclear dust (C). (3) Chaotic nuclear spirals (CS). (4) Loosely Wound nuclear spirals (LW). (5) Tightly Wound nuclear spirals (TW). (6) Grand designed nuclear spirals (GD).

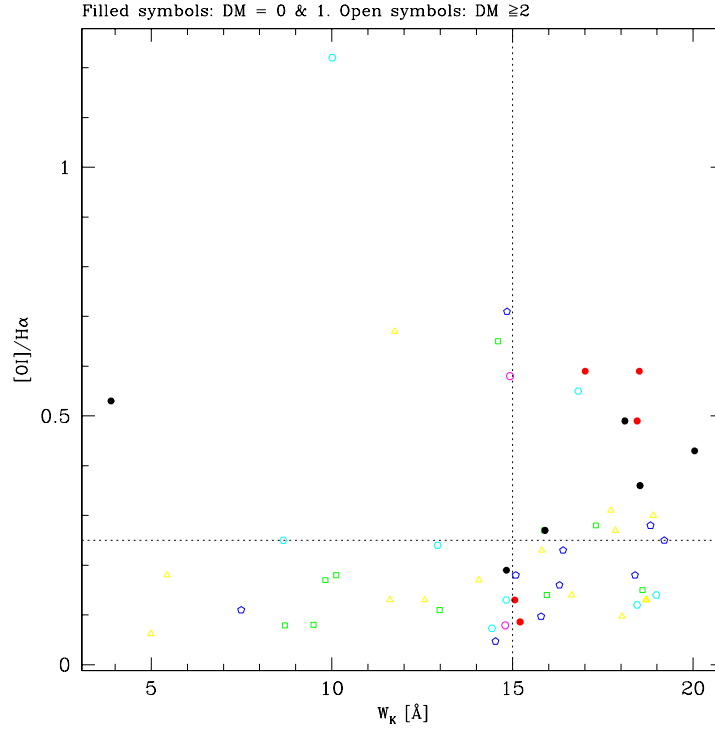


Fig. 6.— The $[OI]/H\alpha$ ratio vs. equivalent width of the CaII K line, W_K . Filled symbols are the LLAGNs with dust morphology belonging to the 'no-dust' or 'dusty-disk' morphologies, open symbols represent LLAGNs with any other type dust morphology. No Young LLAGN falls in either the 'no dust' or 'dusty-disk' classes, but old systems span the whole range of dust morphologies. Note that the only filled symbol with $W_K \leq 15$ Å correspond to NGC 3998 that is an Old LINER.

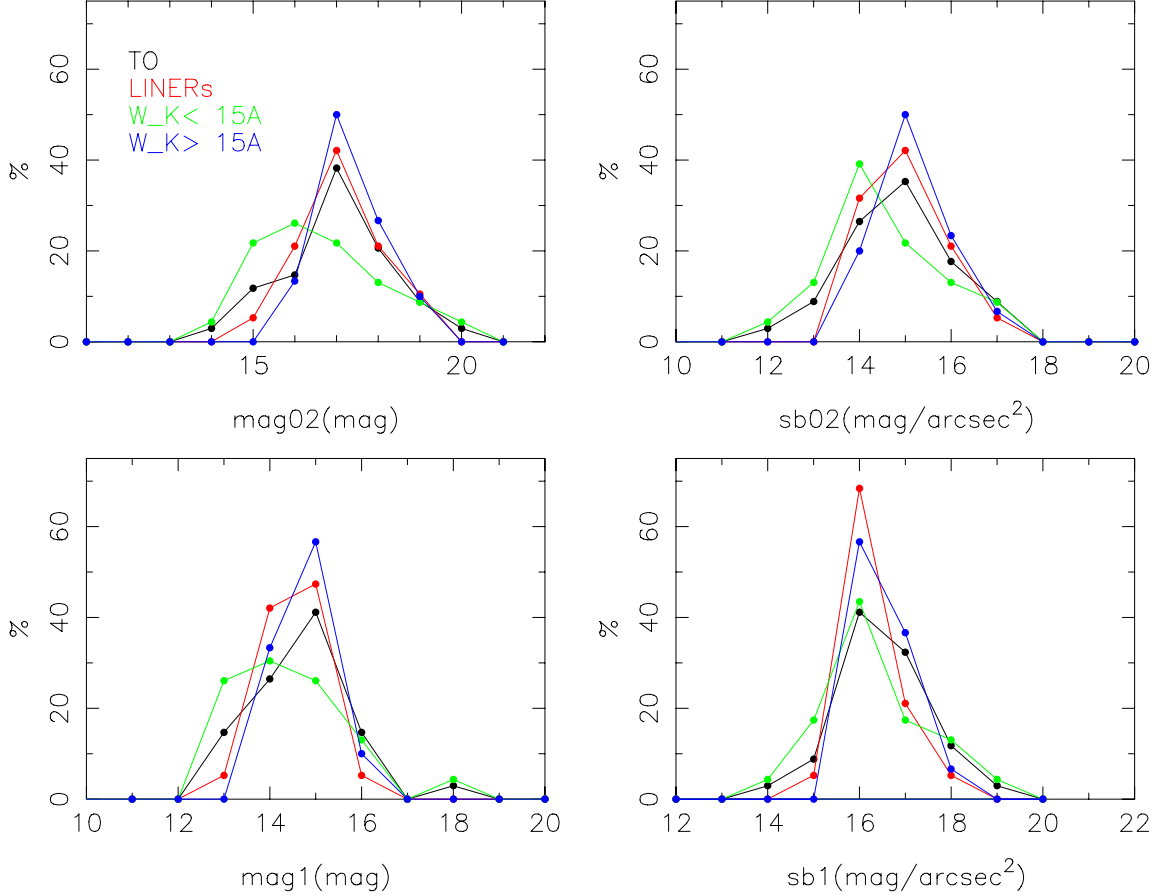


Fig. 7.— Distribution of the magnitude and the surface brightness in the F547M, F555W, or F606W bands. These distributions are plotted for TOs (black), Liners (red), LLAGNs with $W_K \leq 15\text{\AA}$ (green) (they are presumably LLAGNs with young stellar population) and LLAGNs with $W_K > 15\text{\AA}$ (blue). Note that these magnitudes have not been corrected by internal dust obscuration. However, we expect a larger split between the real distributions of LLAGNs with young stellar population and LLAGNs with $W_K > 15\text{\AA}$ if the former sources are the dustier as we estimated in Paper III.

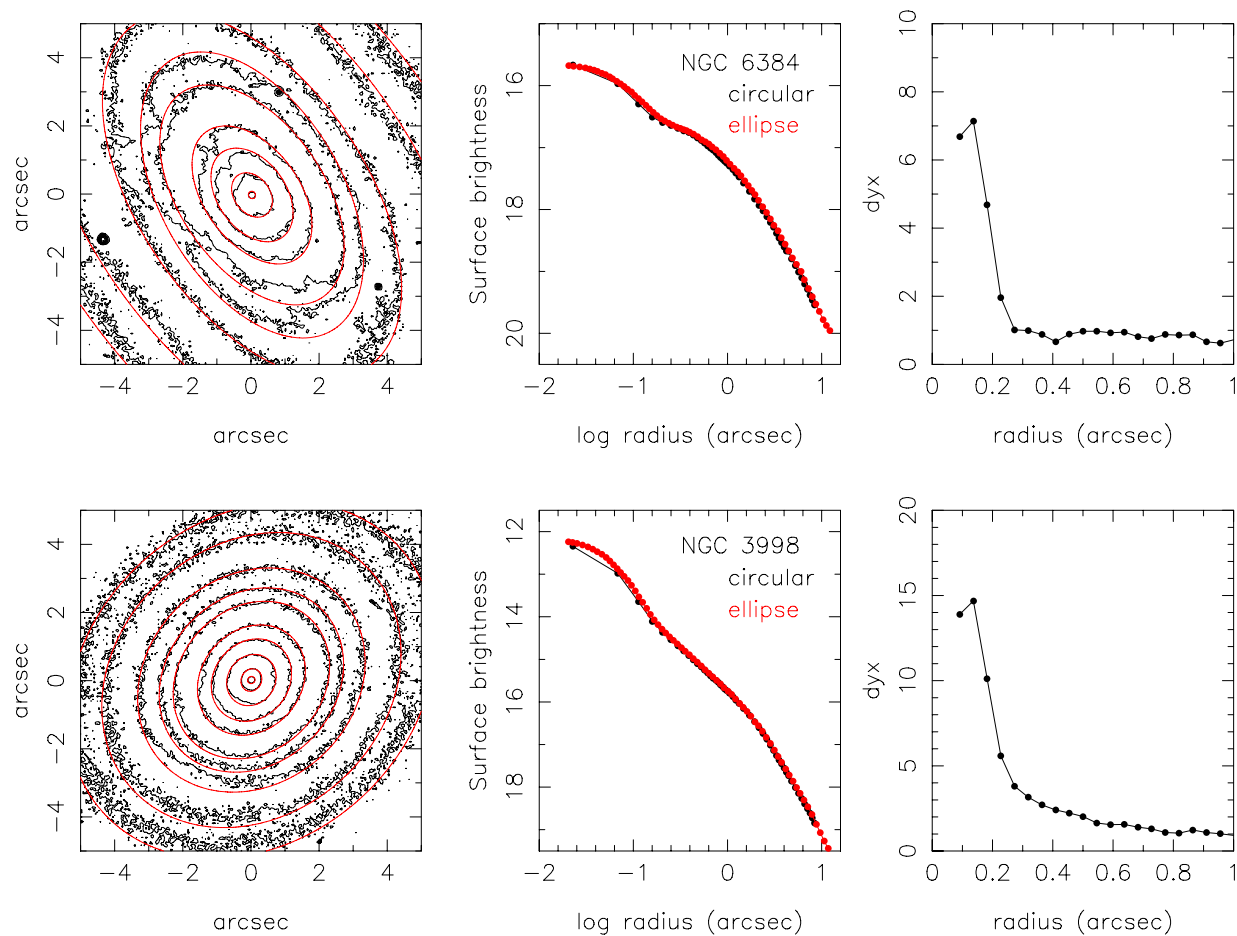


Fig. 8.— Two examples (NGC 3998 (lower panels) and NGC 6384 (upper panel) that illustrate the process followed to identify LLAGNs with nuclear compact sources. Left: The isophotes obtained fitting ellipses (red) to the data (black). Center: Surface brightness obtained with the circular aperture photometry (black) and fitting ellipses (red). Right: gradient of the surface brightness obtained for the profile derived from the circular aperture photometry.

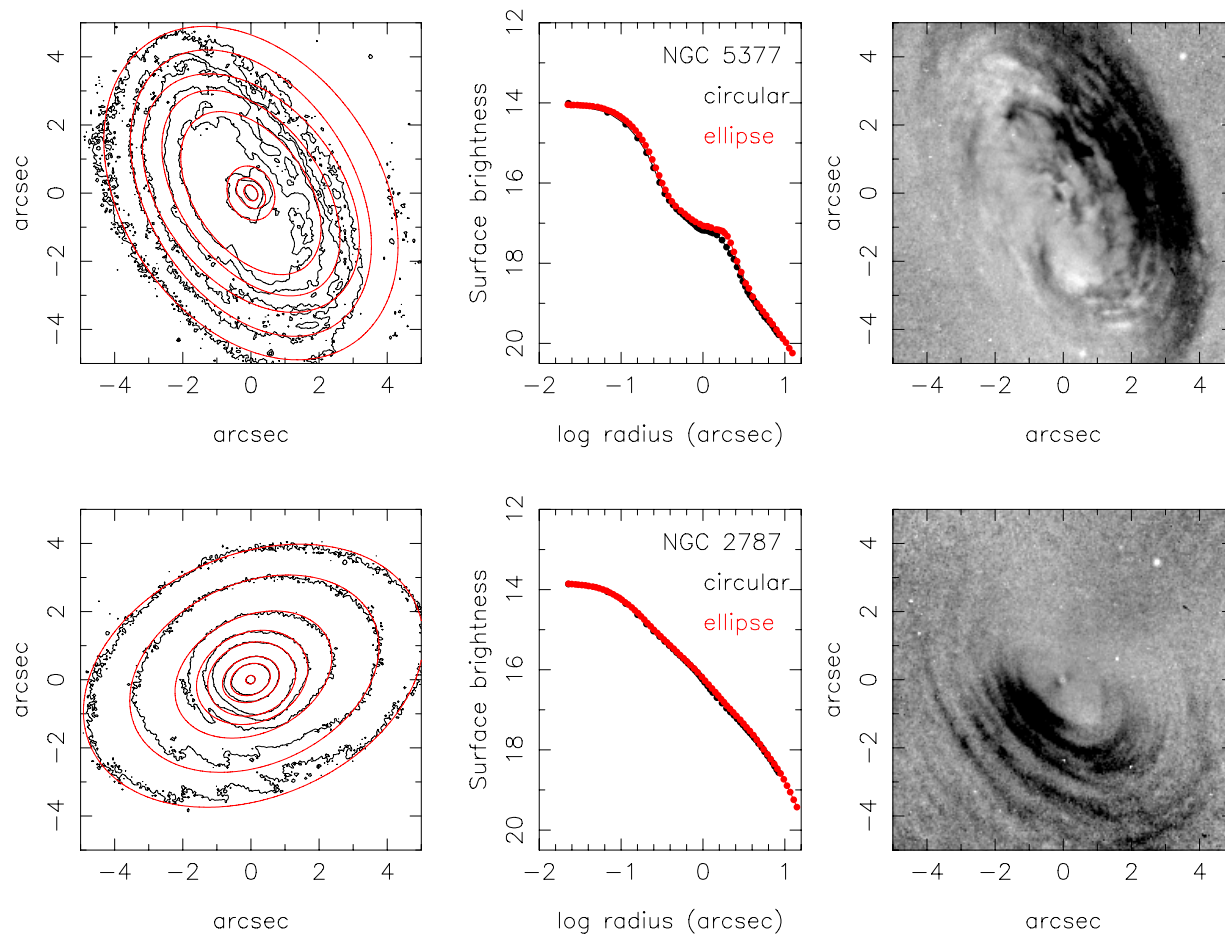


Fig. 9.— Two examples of the isophotal analysis done (left panels), the surface brightness profiles (center panels), and dust obscuration map (right panels). The results are for NGC 5377 (upper panels) and NGC 2787 (lower panels). Left panels compare the galaxy isophotes (black lines) and the isophotal fits (red line). In the center panels, the surface brightness derived from the elliptical isophotal modeling (red points) is compared with the profile obtained using aperture photometry (black points). In the dust maps, the obscuration zones are in black.

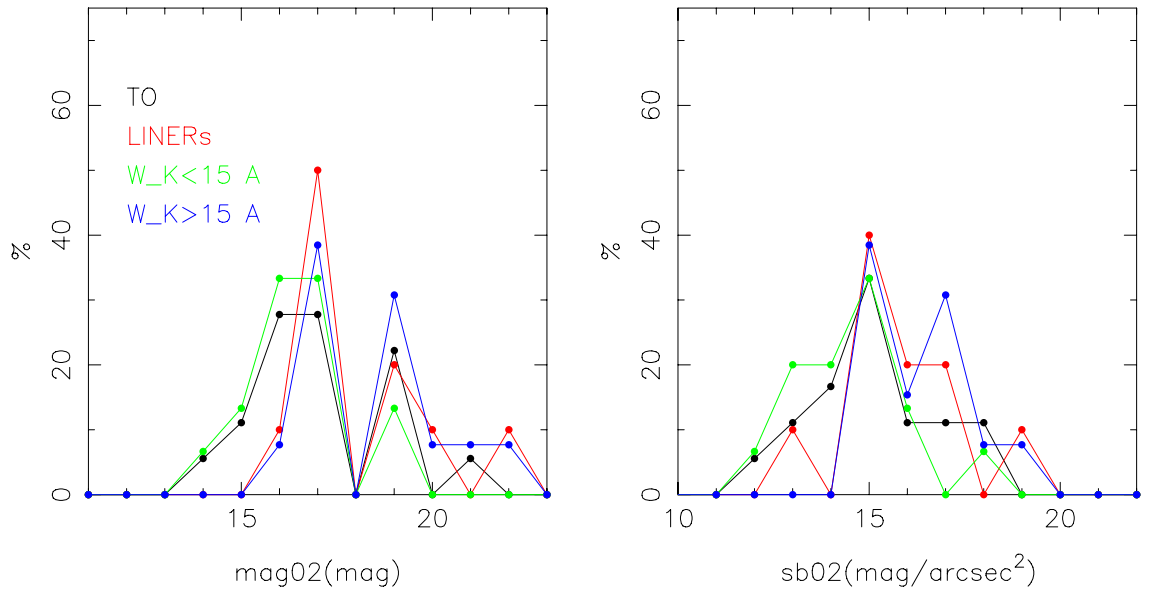


Fig. 10.— Distribution of the nuclear magnitude in the V band. The distribution is plotted for TOs (black), Liners (red), LLAGNs with $W_K \leq 15 \text{ \AA}$ (green) (they are presumably LLAGNs with young stellar population) and LLAGNs with $W_K > 15 \text{ \AA}$ (blue).

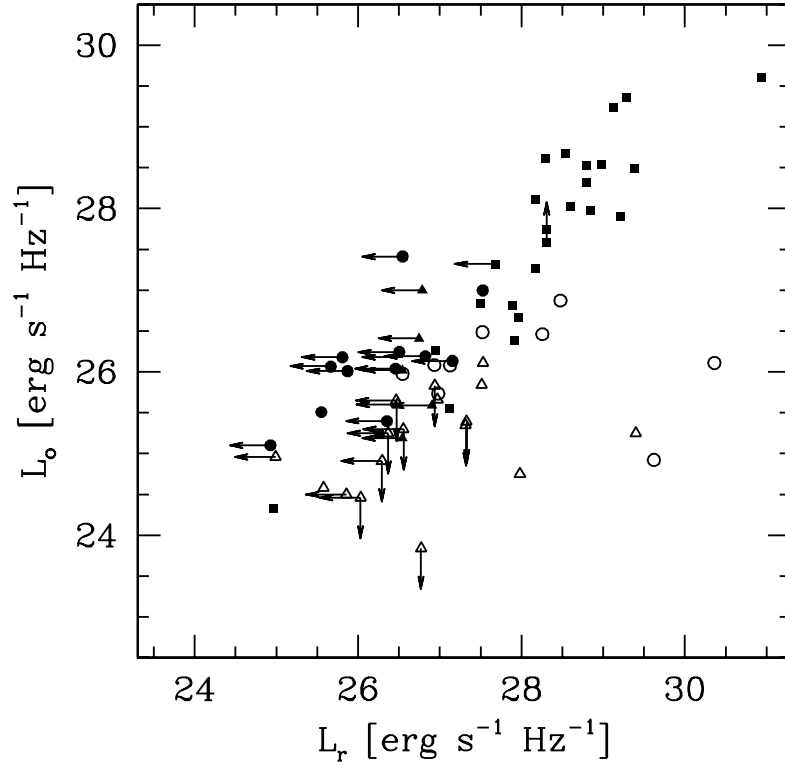


Fig. 11.— Comparison between the optical (7000 Å) and radio (5 GHz) luminosities of Seyfert galaxies (squares) and LINER's (open triangles) from Chiaberge et al. (2005), with our measurements. Old-LINER's are presented as open circles, Old-TO's are presented as filled triangles, and Young-TO's are presented as filled circles.